

Chapter 15

What Can Be Learnt from a Location of Bond Paths and from Electron Density Distribution

Slawomir J. Grabowski

Abstract A bond path being a line of maximum electron density linking attractors of two atoms is often applied in various studies as a criterion of the existence of numerous interactions such as for example hydrogen, halogen or pnictogen bond. It covers cases of atom-atom energetically stabilized links, from weak van der Waals interactions, through stronger Lewis acid–Lewis base interactions up to covalent bonds. The location of bond paths also allows interpreting mechanisms of interactions and, in general, of chemical reactions. The Quantum Theory of Atoms in Molecules (QTAIM) results are mainly presented here; however they are supported by other approaches as, for example, the Natural Bond Orbitals (NBO) method or the σ -hole concept. The most important orbital-orbital interactions determined from the NBO method and characterizing different types of interactions are presented. The analysis of the distribution of the electron charge density is also performed here for numerous systems; this is shown that the regions of the concentration and depletion of the electron density coincide with the regions of the negative and positive regions of the electrostatic potential. The role of the analysis of the laplacian of the electron density is shown on the basis of numerous interactions.

Keywords Bond path • Bond critical point • Laplacian of the electron density • Hydrogen bond • Halogen bond • Pnictogen bond • Lewis acid–Lewis base interaction • Quantum Theory of Atoms in Molecules (QTAIM) • Natural Bond Orbitals (NBO) method • σ -hole concept • Electrostatic potential

S.J. Grabowski (✉)

Kimika Fakultatea, Euskal Herriko Unibertsitatea UPV/EHU, and Donostia International Physics Center (DIPC), P.K. 1072, 20080 Donostia, Euskadi, Spain
e-mail: s.grabowski@ikerbasque.org

S.J. Grabowski

Basque Foundation for Science, IKERBASQUE, Maria Diaz de Haro 3,
48013 Bilbao, Spain

15.1 Introduction

The analysis of the electron charge density is one of the most often applied and standard approaches to describe the system investigated; molecule, ion, greater cluster or even crystal [1–3]. This is why the Quantum Theory of Atoms in Molecules (QTAIM) seems to be a useful tool for such analysis since it concerns directly the electron charge density distribution of the system analyzed [4, 5]. One of ideas of the QTAIM approach is the partitioning of 3D electron charge density space into fragments attributed to atoms (atomic basins); the properties of those fragments are often transferable from one system to another one. In such a way it is possible to consider volumes of atoms or to calculate charges integrated over those volumes. This is important that the mentioned here theoretically calculated volumes and charges may have experimental equivalents since it is possible to perform the crystal structure determination to have the experimental electron charge density distribution in crystal and further apply the QTAIM approach [1–3].

However that is not all; the detailed properties of the electron density, $\rho(r)$, of the system considered may be analyzed [5–7]. The critical points (CPs) denoted by the coordinates r_C , are those where the gradient of the electron density, $\nabla\rho(r_C)$, vanishes and they correspond to minima, maxima or saddle points of the electron density. The CP is labeled by giving the duo of values (ω, σ) , where ω is the rank of CP while σ is its signature. There are the following critical points; $(3, -3)$ —the local maximum often named as attractor is attributed to the position of atom, $(3, -1)$ —the saddle point which often is called the bond critical point (BCP), $(3, +1)$ —the saddle point which is called the ring critical point (RCP) and $(3, +3)$ —the local minimum, i.e. the cage critical point (CCP). The physical interpretation of critical points mentioned here is very well known and it is discussed in numerous monographs and review articles. This is important to announce here that the positions of $(3, -3)$ critical points (attractors) are attributed to the positions of atoms. However there is an excellent agreement between the positions of non-hydrogen attractors and the corresponding nuclei (at least the differences are much smaller than the experimental or theoretical errors) but there is noticeable disagreement between the positions of hydrogen atom attractors (local maxima of the electron density) and their nuclei [8]. This is later discussed in this chapter.

There is another important term useful to describe the distribution of the electron density—the bond path which links pair of attractors [9, 10]. The two gradient paths which originate at the bond critical point and terminate at each of the two attractors define the bond path [11]. In other words the bond path (BP) is a line of the maximum electron density linking the nuclei (more precisely attractors) of two atoms. The bond critical point is that one at the bond path where the electron density attains the minimum value. There are numerous studies on properties and physical meaning of the bond path. It was pointed out that every bond path is accompanied by a virial path [12]. The latter one is a line linking the same nuclei as those connected by the bond path. The virial path is characterized by the maximally negative potential electron energy density thus it is maximally stabilizing with

respect to any other neighboring lines. Bader has pointed out that “one may define a bond path operator as a Dirac observable, making the bond path the measurable expectation value of a quantum mechanical operator” [10]. The bond path denotes two atoms are bonded and it is not equivalent to the chemical bond [10]. The former term can describe the complete range of bonded interactions and is attributed to the electron charge accumulation between the pair of atoms, on the other hand the latter term—bond is limited and dominated by the pair-electron concept of Lewis. This is why the term “bond path” at least should be considered as an alternative way to describe the arrangement of atoms in the species analyzed. This is discussed in the next section.

The molecular graph is defined as a set of bond paths and critical points [6, 7]. Figure 15.1 shows the molecular graph of the complex of water with fluorobenzene. One can observe here the bond paths indicating covalent bonds (solid lines) of the fluorobenzene and water molecules as well as two bond paths indicating intermolecular interactions (broken lines); i.e. the H...F and H...O contacts corresponding to the O–H...F and C–H...O hydrogen bonds, respectively. The isolines of the laplacian of electron density, $\nabla^2\rho^2(r)$, are also presented in this figure and it is

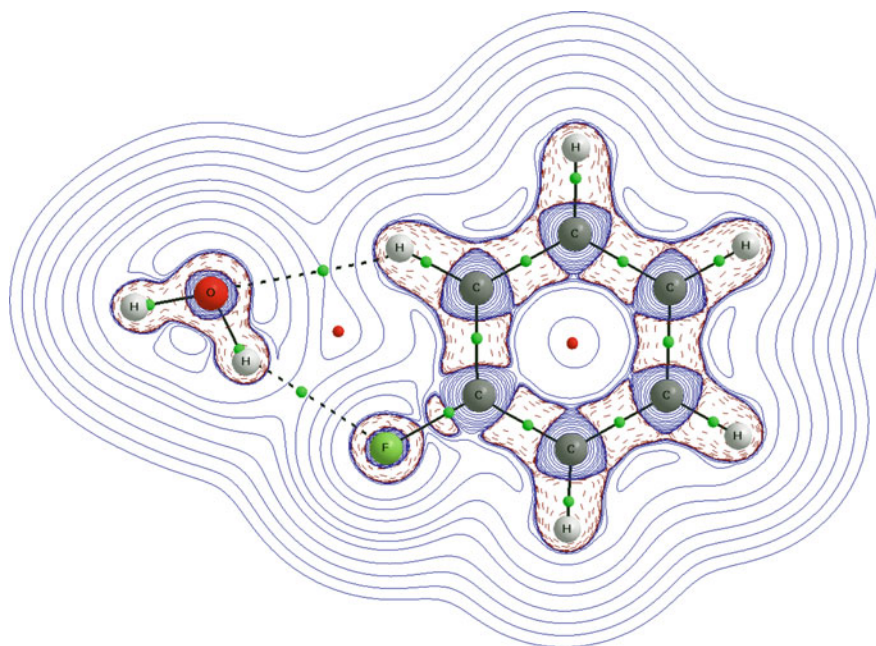


Fig. 15.1 The molecular graph of the $C_6FH_5-H_2O$ complex, solid and broken lines correspond to bond paths, big circles to attractors and small circles to critical points (green—bond critical points, red—ring critical points), the isolines of laplacian of electron density are also presented; positive values are depicted in solid lines and negative values in broken lines (this is the rule for the other figures of this chapter); the laplacian isodensity lines in the plane of the complex; based on the MP2/aug-cc-pVTZ results of calculations

indicated where the laplacian value is negative or positive. The latter indication is useful to describe different characteristics of the system analyzed such as the Lewis acid and Lewis base sites, the nature of interatomic contacts (bonds or intermolecular contacts), the regions of the concentration and depletion of electron charge density—the latter often leads to the location of unshared electron pairs, to the identification if the bond is ionic or covalent in nature, etc. [13–15]. For numerous molecular graphs analyzed hereafter these laplacian isolines or the reactive surfaces ($\nabla\rho^2(r) = 0$ isosurfaces) are also presented to deepen the understanding of the nature of interactions.

There is no difference if, from classical point of view, the intermolecular interaction or the chemical bond is considered. For both cases the bond path is created what means that two atoms are bonded (but it does not mean that necessarily there is the bond between them). Sometimes the characteristics of the bond critical point (BCP) related to the bond path considered are analyzed, the negative value of the laplacian of the electron density at BCP, $\nabla^2\rho_{\text{BCP}}$, indicates the concentration of the electron charge density in the inter-atomic region what is typical for covalent bonds. If the positive value of $\nabla^2\rho_{\text{BCP}}$ is observed thus there is the closed-shell interaction like in a case of an ionic bond, a van der Waals interaction or a hydrogen bond. However the above classification is not always a rule. Sometimes for strong hydrogen bonds the total electron energy density at BCP, H_{BCP} , is negative or even for very strong hydrogen bonds the $\nabla^2\rho_{\text{BCP}}$ value is negative like for the typical covalent bonds [16, 17]. It was stated that the interaction is covalent in nature or at least it is characterized by the partial covalency if H_{BCP} for the analyzed interatomic contact is negative, there is no requirement of the negative value of $\nabla^2\rho_{\text{BCP}}$ [18, 19]. One can mention here well known relationships between energetic topological parameters and the laplacian of the electron density at BCP (expressed in atomic units, see Eq. 15.1) [5, 6].

$$1/4\nabla^2\rho_{\text{BCP}} = 2G_{\text{BCP}} + V_{\text{BCP}}, \quad \text{where } H_{\text{BCP}} = V_{\text{BCP}} + G_{\text{BCP}} \quad (15.1)$$

G_{BCP} and V_{BCP} are the components of the mentioned above H_{BCP} energy density and represent the kinetic electron energy density and the potential electron energy density, respectively. G_{BCP} is always a positive value while V_{BCP} is always negative.

For the $\text{C}_6\text{FH}_5\text{-H}_2\text{O}$ complex presented here the typical medium in strength or weak hydrogen bonds are created where both H_{BCP} and $\nabla^2\rho_{\text{BCP}}$ values are positive. The electron density at the $\text{H}\dots\text{F}$ BCP, ρ_{BCP} , corresponding to the $\text{O-H}\dots\text{F}$ hydrogen bond is equal to 0.014 au while the ρ_{BCP} value for the $\text{H}\dots\text{O}$ contact of the $\text{C-H}\dots\text{O}$ hydrogen bond is equal to 0.009 au. The electron density at BCP corresponding to intermolecular contact, especially in a case of hydrogen bonds, is often treated as the measure of the strength of interaction [16, 17]. The presented values of ρ_{BCP} indicate that the hydrogen bonds considered here are rather weak, for example the ρ_{BCP} for the $\text{H}\dots\text{O}$ intermolecular contact for water dimer linked through the medium in strength $\text{O-H}\dots\text{O}$ hydrogen bond amounts ~ 0.02 au (this value depends slightly on a level of calculations) [20].

It was pointed out that the $n(\text{B}) \rightarrow \sigma_{\text{AH}}^*$ orbital-orbital interaction may be treated as a signature of the $\text{A}\cdots\text{H}\cdots\text{B}$ hydrogen bond since it corresponds to the $\text{H}\cdots\text{B}$ contact [21–24]. For the hydrogen bonds the latter orbital-orbital interaction energy is the most important contribution to the charge transfer energy term. For two $\text{O}\cdots\text{H}\cdots\text{F}$ and $\text{C}\cdots\text{H}\cdots\text{O}$ hydrogen bonds presented in Fig. 15.1 there are the $n(\text{F}) \rightarrow \sigma_{\text{OH}}^*$ and $n(\text{O}) \rightarrow \sigma_{\text{CH}}^*$ orbital-orbital interactions, respectively, with the corresponding energies amounting 1.7 and 0.8 kcal/mol (HF/aug-cc-pVTZ//MP2/aug-cc-pVTZ level). The corresponding $n(\text{O}) \rightarrow \sigma_{\text{OH}}^*$ orbital-orbital interaction for the mentioned above water dimer is equal to ~ 6 kcal/mol (depending on the level of calculation).

One can see two ring critical points (RCPs, red small circles in Fig. 15.1) attributed to the benzene ring and to the ring created by covalent bonds and two $\text{H}\cdots\text{F}$ and $\text{H}\cdots\text{O}$ contacts; i.e. the latter RCP corresponds to the $\text{O}\cdots\text{H}\cdots\text{F}\cdots\text{C}\cdots\text{H}\cdots\text{O}$ ring. Figure 15.1 shows also the isolines of the laplacian of electron density with the regions of the concentration of the electron density at O and F proton acceptor centers. Those regions correspond to the lone electron pairs which are responsible for the existence of the negative electrostatic potentials (EPs) at the oxygen and fluorine atoms. The hydrogen atoms of the $(\text{C})\text{H}\cdots\text{O}$ and $(\text{O})\text{H}\cdots\text{F}$ contacts are characterized by the positive EPs due to the significant outflow of the electron density from the hydrogen atoms to the carbon and oxygen atoms and to the $\text{C}\cdots\text{H}$ and $\text{O}\cdots\text{H}$ inter-atomic regions. Figure 15.2 presents maps of the

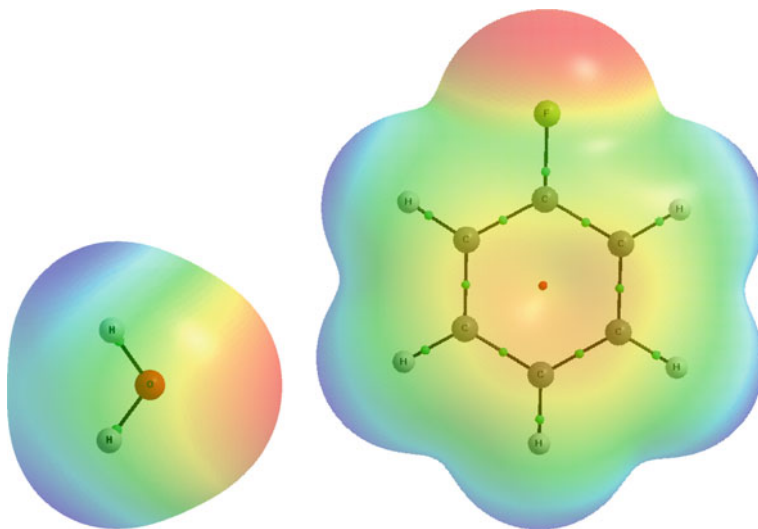


Fig. 15.2 The maps of the electrostatic potential calculated at the 0.001 au molecular electron density surfaces for H_2O (left) and $\text{C}_6\text{H}_5\text{F}$ (right) molecules; red and blue colors correspond to negative and positive EP, respectively. The maximum and minimum EP-values for H_2O are equal to +0.0709 au (H-atoms) and -0.0514 au (O-atom), respectively; such values for $\text{C}_6\text{H}_5\text{F}$ are equal to +0.0296 au (H-atoms) and -0.0259 au (F-atom); MP2/aug-cc-pVTZ level of calculations

electrostatic potential for the H_2O and $\text{C}_6\text{H}_5\text{F}$ molecules calculated separately at 0.001 au electron density molecular surfaces. The distributions of the EP for both species are in line with the observations presented earlier here and concerning the electron charge distribution.

There is another interesting observation for the $\text{C}_6\text{H}_5\text{F}-\text{H}_2\text{O}$ complex (Fig. 15.1). For all O–H, C–H and C–C covalent bonds one can see the continuous regions of the negative laplacian surrounding the corresponding bond critical points; with one exception of the C–F bond where there is the region of positive laplacian between two corresponding nuclei; even the positive $\nabla^2\rho_{\text{BCP}}$ value is detected for the C–F bond critical point. This may indicate that the C–F bond is mostly ionic in nature and that there is the polarization of C–F bond with the concentration of the electron charge density at the fluorine centre. The polarization of C–F bond (the percentage of the electron charge density calculated at F-centre) evaluated within NBO approach is equal to 72.8 %. The QTAIM integrated charges of carbon and fluorine in this bond are equal to +0.472 au and –0.714 au, respectively.

The aim of this chapter is to show, on the basis of several examples, how the location of the bond path may be useful to characterize, define and/or verify the specific, considered interaction. Mainly the QTAIM approach [4–7] is considered here; however sometimes there are also references to other methods and concepts as for example; the Natural Bond Orbitals (NBO) method [21, 22] or the σ -hole concept [25–27]. This is worth to note that the results presented hereafter are mainly based on the MP2/aug-cc-pVTZ level of calculations; those results are taken from earlier studies or the calculations were carried out especially for the purposes of this chapter. Consequently the QTAIM calculations were performed on the MP2/aug-cc-pVTZ wave functions. The binding energies (E_{bin} 's) were calculated as differences between the energy of the complex and the sum of energies of monomers optimized separately and they were corrected for the basis set superposition error (BSSE) by the counterpoise method [28]. Since the NBO method is based on the Hartree-Fock method thus the corresponding NBO results, i.e. orbital-orbital interactions or atomic charges, if presented, are based on the HF/aug-cc-pVTZ//MP2/aug-cc-pVTZ level. Hence there is rather not indicated the level of calculations for the next systems discussed hereafter; unless the results presented were obtained within other levels of calculations.

15.2 The Case of Halogen Bond

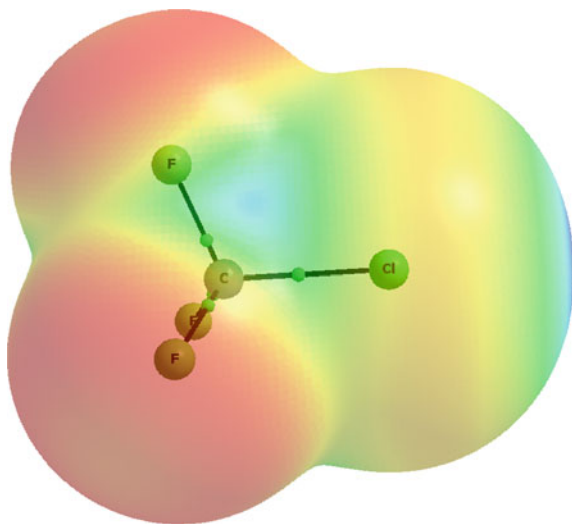
The halogen bond interaction is one of the most interesting phenomena analyzed during the last few decades. It was found that the halogen atoms (designated later here as X), especially if connected with carbon (in C–X bonds), often play a role of electron acceptors (Lewis acid centers) interacting with the Lewis bases, i.e. with the electron rich species. This seems to be strange since halogen atoms are commonly known as the electronegative centers. There were various trials to explain

this phenomenon. One can mention concepts of the anisotropy of the van der Waals radii of halogens [29] or of the anisotropy of the electron charge distribution around the halogen atoms [30]. According to the latter concept the electron density distribution of the halogen atom is characterized approximately by the ellipsoid shape, the major axis of the ellipsoid is perpendicular to the C–X bond while the minor axis belongs to the C–X bond line. This is why the X-centre interacts with nucleophiles in the direction being the elongation of the C–X bond while electrophiles interact with halogens in the direction perpendicular to the C–X bond or nearly so. The latter direction is rich in electron density while the elongation of the C–X bond is characterized by the deficiency of the electron density. These explanations are in line with experimental findings; especially those based on the crystal structures determinations [31].

It seems that more recent σ -hole concept [25–27], being in line with explanations based on the anisotropy of the electron charge distribution, explains additionally the source of such anisotropy as well as this concept explains sufficiently the phenomena of numerous other interactions, not only of the halogen bond. The σ -hole concept of Clark, Murray and Politzer is based on simple models of electron configurations and hybridizations [32, 33]. For example, in a case of the CF_3X molecules ($\text{X} = \text{Cl}, \text{Br}$ and I) the approximate $s^2p_x^2p_y^2p_z^1$ configuration is observed for X-atoms, where the Z-axis is along the C–X bond. The unshared electron pairs are responsible for the existence of the negative electrostatic potential (EP) around the X-atom in the direction approximately perpendicular to the C–X bond while the single p_z^1 electron is involved in the C–X σ -bond what results in the loss of the electron density on the outermost portion of the halogen surface, in the elongation of the C–X bond. This is why this region (σ -hole) is characterized by the positive EP.

Figure 15.3 presents the map of EP for the CF_3Cl molecule. One can see here regions of the negative EP attributed to the fluorine atoms (red color in Fig. 15.3) as

Fig. 15.3 The map of the electrostatic potential calculated at the 0.001 au molecular electron density surface for CF_3Cl molecule; red and blue colors correspond to negative and positive EP, respectively



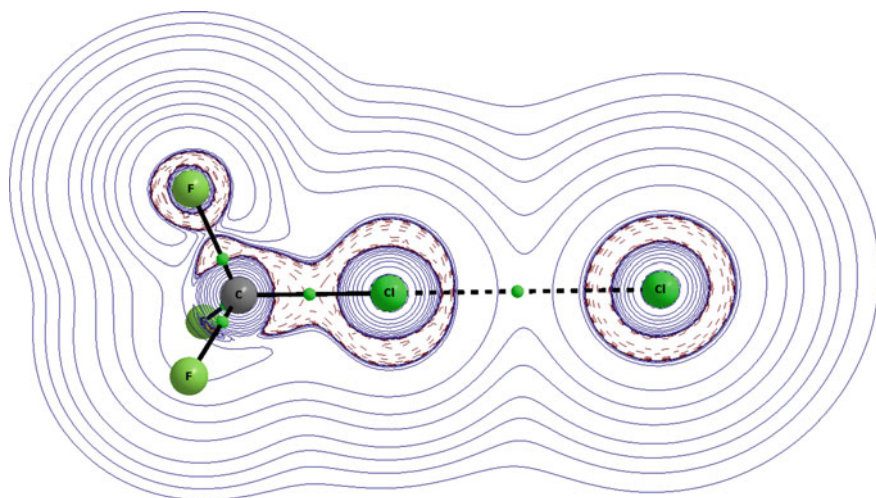


Fig. 15.4 The molecular graph of the $\text{CF}_3\text{Cl}\dots\text{Cl}^-$ complex, solid and broken lines correspond to bond paths, big circles to attractors and small green circles to BCPs, the isolines of laplacian of electron density are also presented; the laplacian isodensity lines in the plane containing CFCl atoms of the CF_3Cl molecule and Cl^- anion

well as less negative region of EP around the Cl-atom (orange color in Fig. 15.3) being the consequence of the existence of unshared electron pairs. The positive region of EP in the elongation of the C–Cl bond is observed (blue color). This is interesting that there are also regions of the positive EP in the elongation of F–C and Cl–C bonds, attributed to the carbon which may also act as the Lewis acid sites. Such regions are also nicely explained in terms of the σ -hole concept.

In general the σ -hole concept explains satisfactory why the halogen centers possess the dual character; they may act as the Lewis acid and as the Lewis base. In the former case the corresponding interaction is named as the halogen bond and it is usually linear or nearly so due to the location of the restricted area of the positive EP in the elongation of C–X bond.

Different complexes of the CF_3Cl moiety were analyzed recently and the dual character of the chlorine centre was also investigated. Figure 15.4 shows the molecular graph of the $\text{CF}_3\text{Cl}\dots\text{Cl}^-$ complex where the chlorine anion is directed to the positive EP region of the Cl-centre in the CF_3Cl molecule. The linear C–Cl...Cl⁻ link is observed what is in line with the σ -hole concept and the earlier explanations presented here. The bond path linking chlorines with the corresponding BCP is observed. The isolines of laplacian of the electron density are also presented showing the anisotropic concentration of the electron density around the (C)Cl chlorine centre while the unperturbed spherical concentration of the electron density is observed for chlorine anion. One can also see the regions corresponding to other σ -holes, attributed to the carbon, i.e. to the elongations of the F–C and Cl–C bonds.

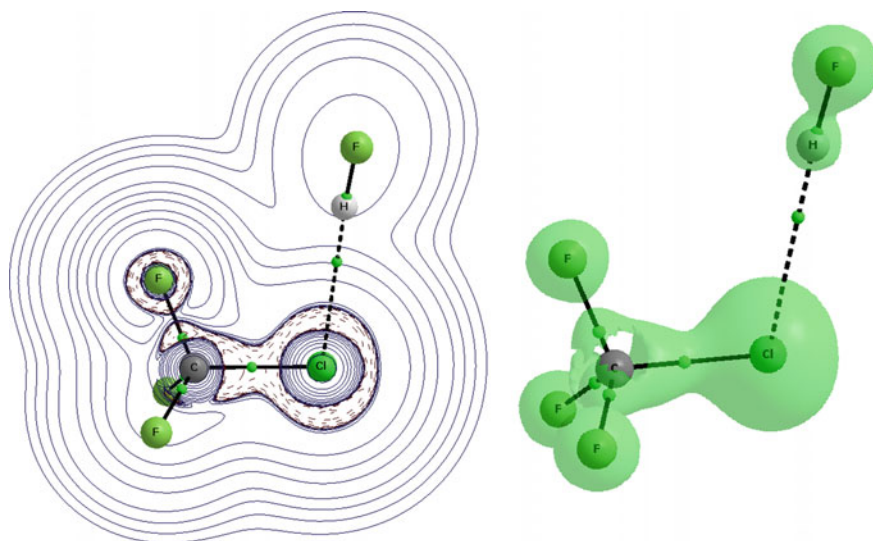


Fig. 15.5 The molecular graph of the $\text{CF}_3\text{Cl}\dots\text{HF}$ complex, *solid* and *broken lines* correspond to bond paths, *big circles* to attractors and *small green circles* to BCPs, the isolines of laplacian of electron density are also presented (the laplacian isodensity lines in the plane containing CFCI atoms of the CF_3Cl molecule); the reactive surface ($\nabla^2\rho(r) = 0$ isosurface) is presented in the *right* part of the figure

Figure 15.5 presents the molecular graph of the $\text{CF}_3\text{Cl}\text{--}\text{HF}$ complex where the positively charged and characterized by the positive EP hydrogen atom of HF is directed to the “belt” of the negative EP around chlorine atom; this “belt” is visible from the map of the laplacian isolines performed in the plane containing CFCI atoms of the CF_3Cl molecule. In other words the Cl-centre plays the role of the Lewis base in this complex. There are other interesting findings here. The HF molecule is situated outside of the mentioned above CFCI plane. This is why the 2D map with laplacian isolines do not show the negative regions of the laplacian for the HF molecule since the latter species is situated outside the molecular graph projection. Probably such a configuration of the complex is observed because of the repulsion between the fluorine atoms of CF_3Cl and the fluorine atom of HF molecule. Figure 15.5 presents also the reactive surface ($\nabla^2\rho(r) = 0$ isosurface); this picture may be read in the following way, the areas closed by those lines are characterized by the negative values of the laplacian of electron density thus they correspond to the concentration of the electron charge.

It was explained in terms of the σ -hole concept that the fluorine usually does not possess the regions of positive EP since the high electronegativity of F-centre as well as the sp -hybridization cause that the σ -hole usually occurring in the outermost part of C–F bond is neutralized [32, 33]. Additionally the Lewis acid strength for halogen atoms increases in the following order, $\text{F} < \text{Cl} < \text{Br} < \text{I}$ what is connected with the increase of the polarization of the corresponding C–X bonds (% of the

electron density calculated at the carbon atom increases). For example, the HCCX halogen derivatives of acetylene were analyzed and it was found that the maximum EP at X center is equal to +2.3, +20.4 and +27.0 kcal/mol for X = F, Cl and Br, respectively (B3PW92/6-31G(d,p) level of calculations) [34]. There are similar findings of an increase of the positive EP for heavier X-center for other species, like for example H_3CX , F_3CX or C_6H_5X [34].

Figure 15.6 presents the molecular graphs of HCCCl and HCCBr molecules with the isolines of the laplacian of electron density. One can see the anisotropic

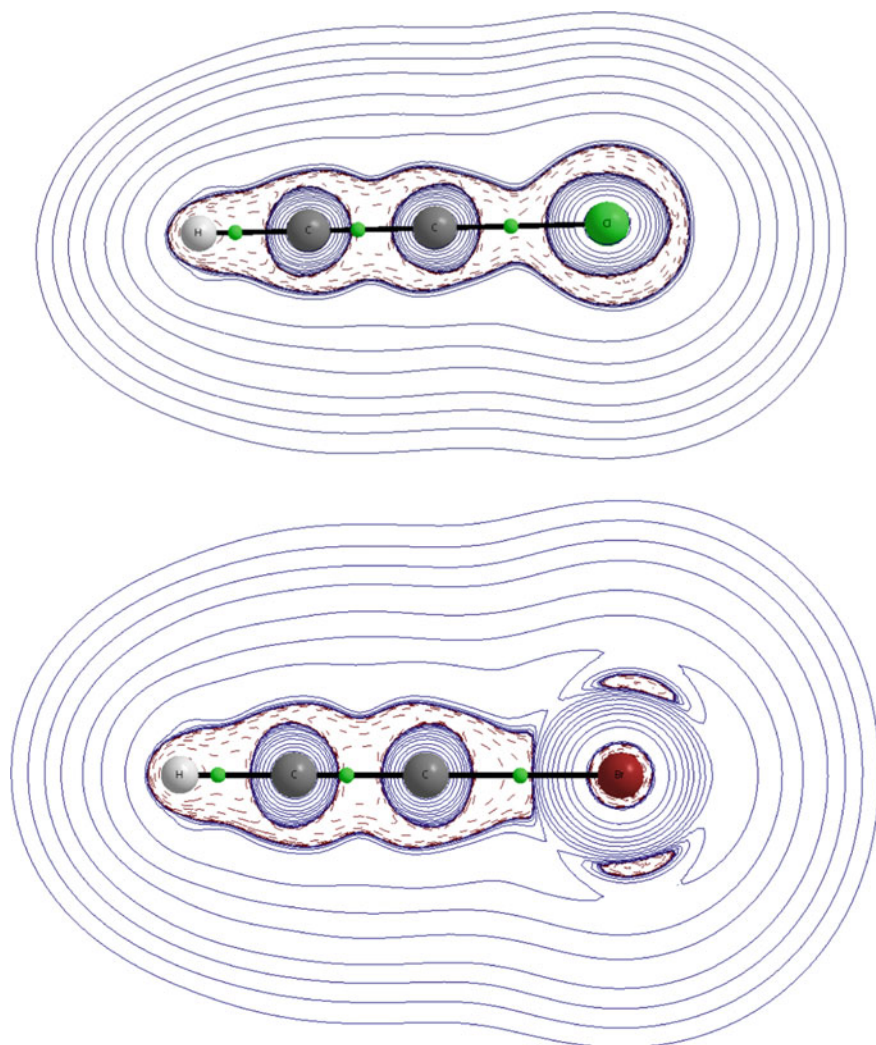


Fig. 15.6 The molecular graphs of the HCCCl (*up*) and HCCBr (*down*) molecule, *solid and broken lines* correspond to bond paths, *big circles* to attractors and *small green circles* to BCPs, the isolines of Laplacian of electron density are also presented

concentration of the electron charge density around chlorine for the HCCCl molecule, with its “thin” concentration in the elongation of C–Cl bond and wider concentration in the direction perpendicular to this bond; the latter corresponds to the lone unshared electron pairs. In a case of HCCBr molecule there is no the concentration of the electron density in the C–Br bond line! This is why the more positive EP is observed for the bromine derivative of acetylene than for the chlorine derivative.

In a case of halogen bond the monovalent halogen center is usually analyzed while there are only few studies on that kind of interaction with multivalent halogen atoms. One can mention the study on Ph_2IX complexes with XF_3 ($\text{X} = \text{Cl}, \text{Br}, \text{I}$) [35] or the study where the complexes of XF_3 are compared with their XF analogues ($\text{X} = \text{Br}$ or Cl) [36]. Very recently the complexes of BrF_3 and BrF_5 with N_2 and HCN species acting as Lewis bases were analyzed [37]. The situation for the bromine center in BrF_3 and BrF_5 is different than in a case of monovalent halogens. First of all, the whole hemispheres of multivalent bromines are characterized by the positive electrostatic potential. It means that bromine should play the role of the Lewis acid only and not of the Lewis base. For the BrF_3 moiety characterized by the C_{2v} symmetry the maximum positive EP occurs for the Br center in the elongation of the F–Br equatorial bond (Fig. 15.7). Slightly different situation is observed for the C_{4v} symmetry BrF_5 molecule where four equivalent maxima of EP are observed at Br-center, around the fourfold symmetry axis of the molecule (Fig. 15.7).

The distribution of the electrostatic potential for two bromine species has further consequences; particularly the location of the maxima of EP shows the most probable nucleophilic attacks here. This is why the liner halogen bonds are formed with BrF_3 while bent ones for the BrF_5 molecule. Figure 15.8 shows the molecular graph of the $\text{BrF}_3\text{--NCH}$ complex with the reactive surface corresponding to the laplacian of the electron density equal to zero. The straight bond path connecting the bromine atom with the nitrogen Lewis base center of HCN molecule is observed

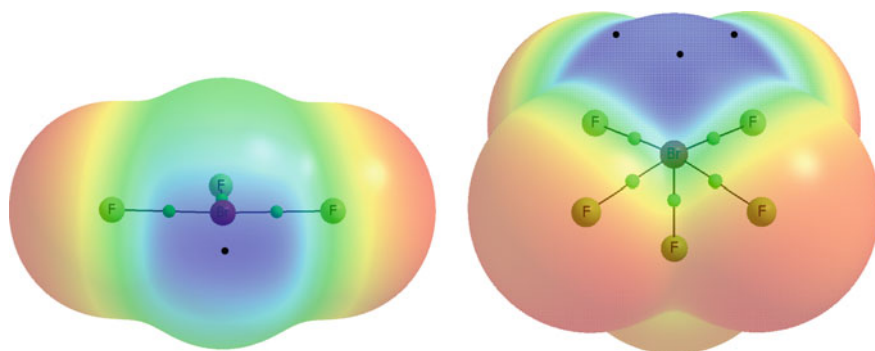


Fig. 15.7 The map of the electrostatic potential calculated at the 0.001 au molecular electron density surfaces for BrF_3 (left) and BrF_5 (right) molecules; red and blue colors correspond to negative and positive EP, respectively. Black points designate the maxima of EP, one local maximum for BrF_3 and 4 local maxima for BrF_5 (only 3 maxima are visible in the figure)

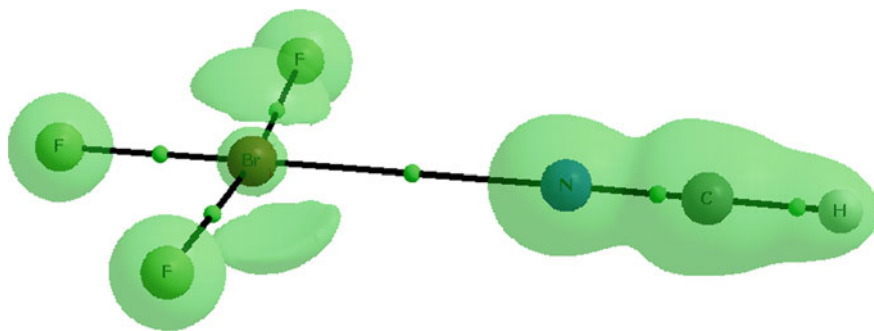


Fig. 15.8 The molecular graph of the $\text{BrF}_3 \dots \text{NCH}$ complex, *solid lines* correspond to bond paths, *big circles* to attractors and *small green circles* to BCPs, the reactive surface ($\nabla^2 \rho(r) = 0$ isosurface) is also presented

here; one can say that the bond path crosses the maximum of EP of the bromine atom. It is worth to mention that the BrF_3 molecule displays a T-shaped molecular structure and a trigonal bipyramidal electronic structure. Two lone unshared electron pairs are located symmetrically to the mirror plane containing the BrF_3 molecule. This picture is in line with the chemical intuition and with the NBO results. The latter approach confirms the existence of two unshared electron pairs for bromine which is also characterized by 14 core orbitals (28 electrons); 3 remaining bromine electrons are involved in Br–F bonds. The electron configurations for bromine in the isolated BrF_3 molecule and in the $\text{BrF}_3\text{--NCH}$ complex are practically the same according to the NBO approach, only there are negligible differences in the occupancies of orbitals.

As it was pointed out earlier here, the different situation is observed for the BrF_5 moiety. For example, for the $\text{BrF}_5\text{--N}_2$ complex the Lewis base N-center of molecular nitrogen is directed to one of the BrF_5 EP maxima. Figure 15.9 presents the corresponding molecular graph of that complex with the $\text{Br} \dots \text{N}$ bond path crossing the local EP maximum and partly avoiding the unshared electron pair of bromine. The bromine electron configuration derived from NBO for the BrF_5 moiety is as follows, 28 core electrons, 1 lone electron pair and 5 remaining electrons are involved in 5 F–Br σ -bonds. This means that for the square pyramidal BrF_5 molecular structure observed here there are 12 electrons in the valence shell. The latter is often named as hypervalency in the literature [38] since the octet rule is not obeyed here. The electron configuration of bromine in the $\text{BrF}_5\text{--N}_2$ complex is practically the same as in the BrF_5 moiety not involved in any interaction, similarly as it was observed in a case of the BrF_3 species and its complexes.

Very interesting situation is observed for the $\text{BrF}_5\text{--Cl}^-$ complex (Fig. 15.10). This complex is characterized by a very strong interaction since the binding energy amounts here -37.8 kcal/mol while for the complexes of BrF_5 with HCN and N_2 the binding energy is equal to -5.1 and -1.7 kcal/mol, respectively [37]. The laplacian of the electron density, $\nabla^2 \rho_{\text{BCP}}$, at Br–Cl BCP is positive; however the

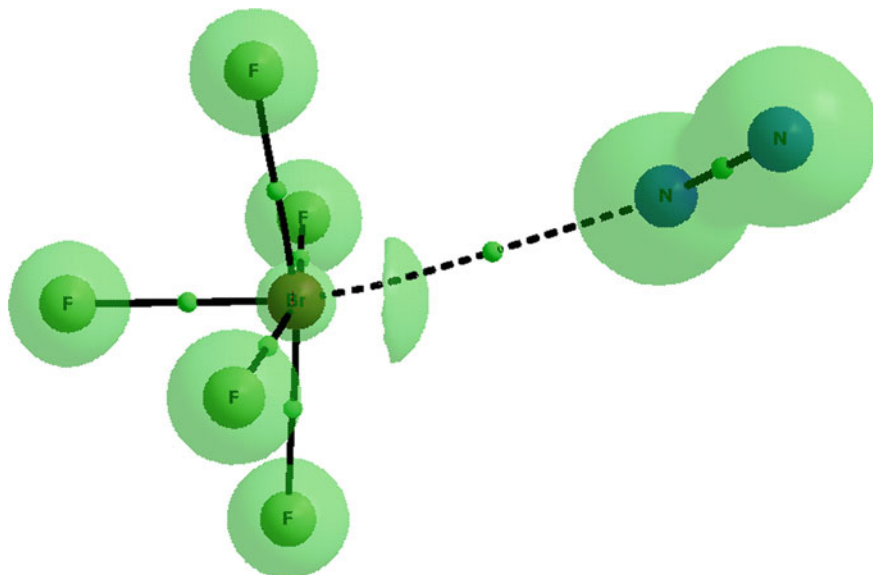


Fig. 15.9 The molecular graph of the $\text{BrF}_5 \dots \text{N}_2$ complex, solid and broken lines correspond to bond paths, big circles to attractors and small green circles to BCPs, the reactive surface ($\nabla^2 \rho(r) = 0$ isosurface) is presented

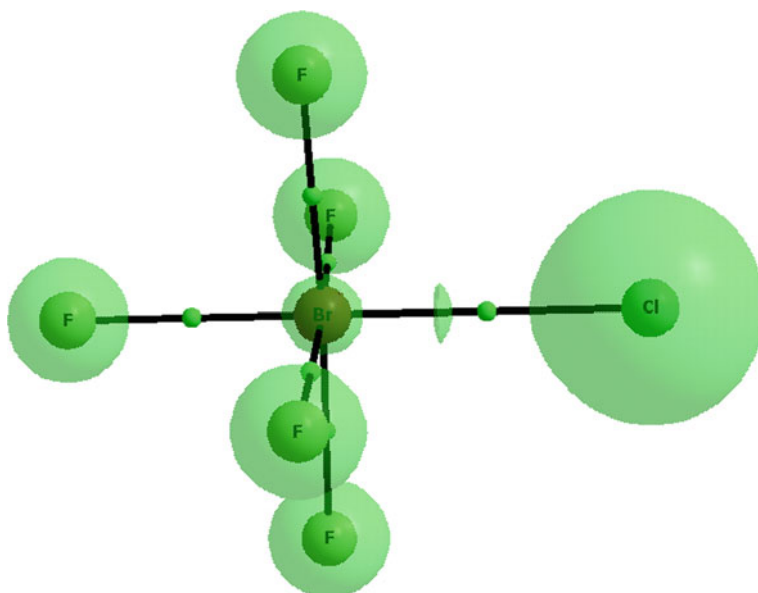


Fig. 15.10 The molecular graph of the $\text{BrF}_5 \dots \text{Cl}^-$ complex, solid lines correspond to bond paths, big circles to attractors and small green circles to BCPs, the reactive surface ($\nabla^2 \rho(r) = 0$ isosurface) is presented

total electron energy density at BCP, H_{BCP} , is negative what means that the interaction is at least partly covalent in nature. The similar situation is observed for all five Br–F connections—the positive $\nabla^2\rho_{\text{BCP}}$ values and the negative H_{BCP} ones. It seems that the strong interaction of the BrF_5 species with the Cl^- anion extorts the greater electron density changes in the complex, particularly in the BF_5 moiety. One lone electron pair of bromine is observed in the complex within the NBO approach, similarly as in the isolated BrF_5 species; however the lone pairs in the complex possesses s-character in 99.2 %. This is confirmed by the QTAIM approach since Fig. 15.10 shows the spherical electron charge density concentration around bromine center. The change of the location of the bromine electron lone pair results in the existence of the straight bond path linking the Br and Cl centers in contrary to the interactions of the BrF_5 molecule with weak Lewis bases (see Fig. 15.9).

The positive values of the laplacian of electron density at all BCPs corresponding to the Br–F and Br–Cl links in the $\text{BrF}_5\text{--Cl}^-$ complex may indicate the ionic character of interactions since it was pointed out that such values are typical for the closed-shell interactions [5–7]. This means that in the latter complex all bonds (links) are strongly polarized; the NBO approach shows that the polarization for the Br–F bonds is equal to 23.2 % and it amounts 33.6 % for the Br–Cl bond (% of the electron density at the Br center). The Br atomic charge calculated within NBO and QTAIM approaches is equal to +2.25 au and +2.32 au, respectively. Figure 15.10 clearly shows the concentration of the electron density at attractors and not at interatomic regions; the similar situation is observed for all BrF_3 and BrF_5 complexes.

There is another interesting finding for the $\text{BrF}_5\text{--Cl}^-$ complex; the NBO approach shows that there are tri-center four-electron (3c-4e) linear bonds here. They concern the following linear triads in the BF_5Cl^- moiety; two F–Br–F triads and one F–Br–Cl triad. Such 3c-4e bonds were analyzed earlier in literature; for example Weinhold and Landis analyzed numerous hypervalent centers [21] and they extended the 3c-4e concept of Pimentel and Rundle [39, 40].

15.3 Lewis Acid–Lewis Base Interactions

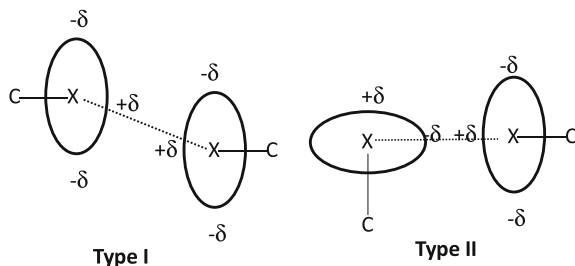
The σ -hole concept mentioned in the previous section which explains the mechanisms of formation of the halogen bond is also useful to analyze other Lewis acid–Lewis base interactions [26, 27, 41]. One can mention tetrel [42–45], pnictogen [46–50] and chalcogen bonds [51–53] where the elements of Groups IV, V and VI, respectively, play the role of the Lewis acid centers. The mechanism of the formation of those bonds is practically the same as that one of the halogen bond; a region of positive electrostatic potential (designated as σ -hole) on the extension of the bond to the atom being the acidic center is an effect of the electron charge shift from the outermost part of this center. These centers possessing σ -holes are usually characterized by the unshared electron pairs thus they may act simultaneously as the Lewis acids and the Lewis bases. The situation is slightly different for the tetrel

atoms which are characterized by the sp^3 hybridization and do not possess free electron pairs. That rather excludes their potential basicity. Similarly, as it was mentioned earlier here in the previous section, multivalent halogens may be characterized only by acidity properties but in that case the halogen centers possess lone electron pairs.

The dual character mentioned few times here results in important consequences that the same elements may be involved in the stabilization interaction; i.e. that halogen-halogen, chalcogen-chalcogen, etc. interactions are possible. That is not all since at least two different in nature connections may be mentioned here. For example, the X halogen center may interact by its Lewis acid region (σ -hole) with the Lewis base region (unshared electron pairs) of the X-center of another molecule or both halogen centers being in the X...X contact may play the dual role, both may act simultaneously as Lewis acid and Lewis base. Both cases of C-X...X-C halogen-halogen interactions were described in early study of Fourmigue and Batali [31] and they are presented in Scheme 15.1. In a case of the interaction designated as I, the halogen atoms act simultaneously as Lewis acid and Lewis base centers. Such centers may be sometimes related by symmetry, for example, in the crystal structures such halogen atoms may belong to symmetry equivalent molecules. In a case of the type II interaction one of halogens acts as the Lewis base and the second one as the Lewis acid in spite of the fact that potentially both possess dual character.

Similar types of interactions are observed for other σ -hole bonds. For example, P...P pnictogen interactions were analyzed in numerous complexes [54, 55]. For the FH_2P-PH_3 complex the σ -hole of the FH_2P moiety situated in the elongation of the F-P bond interacts with the lone electron pair of the PH_3 species; this corresponds to the $n(P) \rightarrow \sigma_{PF}^*$ orbital-orbital interaction within the NBO approach; in other words the FH_2P species reveals here the Lewis acid properties while the PH_3 molecule the Lewis base properties. One can expect the reverse situation, where the FH_2P and PH_3 molecules act as the Lewis base and the Lewis acid, respectively with the corresponding $n(P) \rightarrow \sigma_{PH}^*$ orbital-orbital interaction. However the P center possesses the stronger Lewis acid properties in the FH_2P molecule than in the PH_3 species since the $n(P) \rightarrow \sigma_{PF}^*$ and $n(P) \rightarrow \sigma_{PH}^*$ energies of interactions in the FH_2P-PH_3 complex are equal to 8.9 and 2.7 kcal/mol, respectively. Besides the FH_2P σ -hole (elongation of the F-P bond) is characterized by the more positive EP than the PH_3 σ -hole (elongation of H-P bond) [54, 55]. Figure 15.11 presents the molecular graph of this complex with the reactive surface ($\nabla\rho^2(r) = 0$ isosurface). One can see that two molecules of the complex are oriented in such a way that lone electron pair (the electron charge density concentration) is directed to the σ -hole region.

On the other hand the $(FH_2P)_2$ dimer represents the situation of the equivalent phosphorus atoms, both acting simultaneously as the Lewis acid and as the Lewis base what corresponds to two equivalent $n(P) \rightarrow \sigma_{PF}^*$ orbital-orbital interactions (each characterized by the energy of 29.5 kcal/mol). Figure 15.12 presents the molecular graph of this complex. The authors described also P...P interactions in other complexes [55]; for example for the $FH_2P...P(OH)H_2$ complex there are two important orbital-orbital interactions: $n(P) \rightarrow \sigma_{PF}^*$ and $n(P) \rightarrow \sigma_{P-OH}^*$; however the



Scheme 15.1 Two types of C-X...X-C halogen-halogen interactions; this figure is based on the scheme presented in Ref. [31]; the ellipsoids represent here the non-spherical distribution of the electron charge density

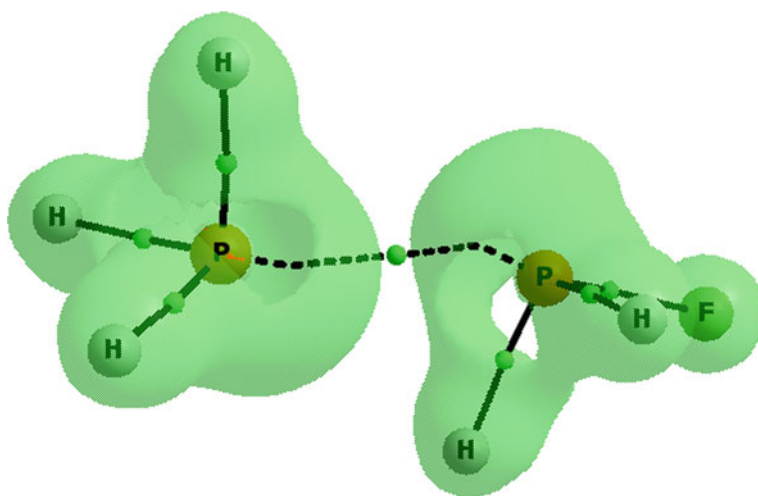


Fig. 15.11 The molecular graph of the $\text{FH}_2\text{P}\dots\text{PH}_3$ complex, solid and broken lines correspond to bond paths, big circles to attractors and small green circles to BCPs, the reactive surface ($\nabla^2\rho(r) = 0$ isosurface) is presented

former one is stronger than the latter one what means that the P center is more acidic in the PFH_2 moiety than in the P(OH)H_2 one.

The results presented here show that for the pnictogen-pnictogen contacts there is no clear border between type I and II configurations as it was found for halogen-halogen interactions (Scheme 15.1). It seems that an orientation corresponding exactly to the II type orientation found for the X...X contacts cannot be formed for the P...P interaction. It probably comes from the existence of three σ -holes for trivalent P centers while in a case of monovalent halogens there is only one σ -hole characterized by the acidic properties.

This is worth mentioning that in both cases of pnictogen-pnictogen interaction there is only one bond path linking the corresponding attractors (see Figs. 15.11 and

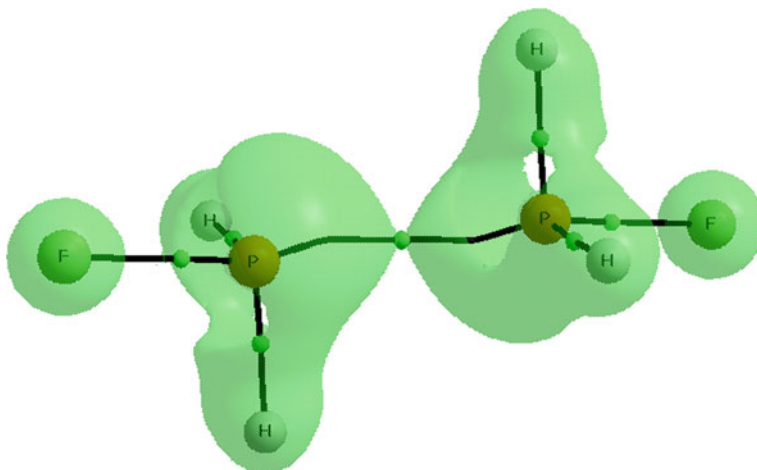


Fig. 15.12 The molecular graph of the $(\text{FH}_2\text{P})_2$ dimer, solid lines correspond to bond paths, big circles to attractors and small green circles to BCPs, the reactive surface ($\nabla^2\rho(r) = 0$ isosurface) is presented

15.12). It seems that this situation may be generalized for interactions between the same kind centers, i.e. for the chalcogen-chalcogen or halogen-halogen (dihalogen) bonds. The results presented here show that the molecular graph does not reflect more complex situation, i.e. differences between those two cases. Such difference is reflected within the NBO analysis. However it seems that the QTAIM approach provides the tools to describe that more complex situation. The σ -hole bonds, i.e. halogen and pnictogen bonds, were analyzed recently by Eskandari and co-workers [56, 57]. They have shown that the P...P, P...N and N...N interactions [56], as well as halogen bonds [57], may be categorized as lump-hole interactions where the hole is a region of charge depletion and the excess of the kinetic energy while the lump is a region of the electron charge concentration and an excess of the potential energy. In such a way the authors have found one hole-lump interaction for the $\text{FH}_2\text{P}\dots\text{PH}_3$ complex and two equivalent hole-lump interactions for the $(\text{FH}_2\text{P})_2$ dimer [56] what corresponds to one dominant or two equivalent orbital-orbital interactions, respectively.

There is a very interesting case of tetrel bonds where the Group IV element plays the role of the Lewis acid center. The tetrel bonds were analyzed recently as a kind of σ -hole bonds [42–45]; however such interactions were known early on as the preliminary stages of the $\text{S}_{\text{N}}2$ reactions [58, 59]. For example, the methane species may be treated as a very weak acid interacting through the H-atom with the Lewis base centre; H-atoms of methane are characterized by the positive EP (+0.015 au at 0.001 au molecular surface) while C-centre by slightly negative EP (−0.004 au). Figure 15.13 presents the molecular graph of the $\text{CH}_4\dots\text{NCH}$ complex corresponding to this situation where the H...N bond path corresponding to the C–H...N hydrogen bond is observed. However for the CH_3Cl derivative there is the region of

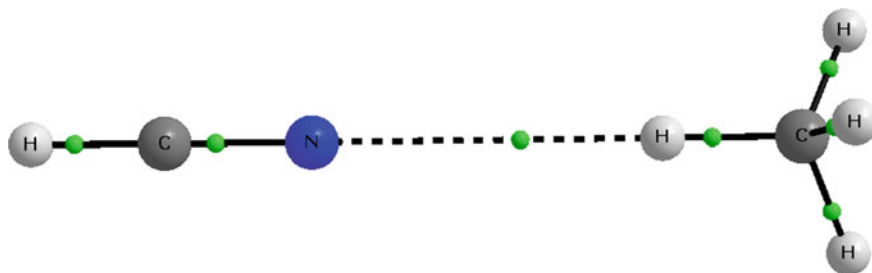


Fig. 15.13 The molecular graph of the $\text{CH}_4 \dots \text{NCH}$ complex, solid and broken lines correspond to bond paths, big circles to attractors and small green circles to BCPs

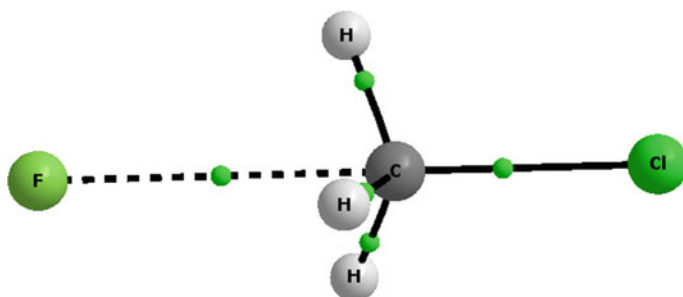


Fig. 15.14 The molecular graph of the $\text{CH}_3\text{Cl} \dots \text{F}^-$ complex, solid and broken lines correspond to bond paths, big circles to attractors and small green circles to BCPs

the positive EP (+0.032 au) at the C-center in the elongation of the Cl–C bond, this is the σ -hole which plays the role of the Lewis acid in interactions with electron rich species. Figure 15.14 presents the molecular graph of such situation; this is the $\text{CH}_3\text{Cl} \dots \text{F}^-$ complex which may be treated as the preliminary stage of the $\text{CH}_3\text{Cl} + \text{F}^- \rightarrow \text{CH}_3\text{F} + \text{Cl}^-$ reaction governed by the $\text{S}_{\text{N}}2$ mechanism.

Let us look at few experimental studies; the addition reactions of methyl(halogeno)tin and methyl(halogeno)germanium compounds to electron-rich platinum(II) complexes were analyzed [60]. These studies clearly point to an $\text{S}_{\text{N}}2$ mechanism for the interactions considered. It was found that methylhalotin species, Me_3SnX ($\text{X} = \text{Cl}, \text{Br}, \text{I}$), react by an $\text{S}_{\text{N}}2$ pathway. The germanium analogues were also analyzed. For example, the variable temperature NMR spectral series for Me_3GeCl shows the rate decrease of the $\text{S}_{\text{N}}2$ reaction in comparison with the analogues tin species and the authors explain that this is partly due to a size effect. This is in line with the σ -hole concept as well as with the topology of complexes linked through the tetrel bonds. It was found that for the tetrel atoms as well as for the other Groups centers the positive EP increases in the Group if the atomic number of the center

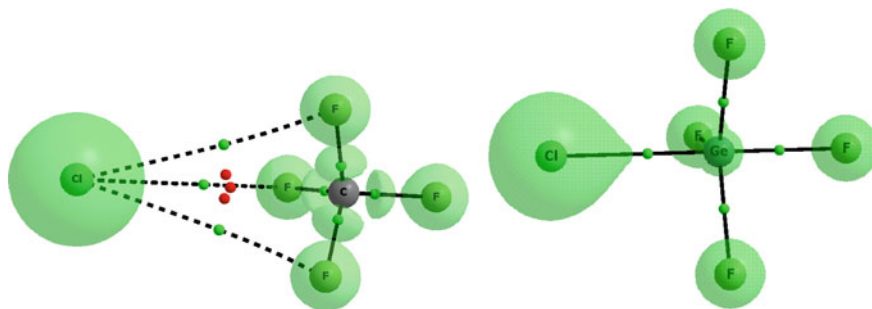


Fig. 15.15 The molecular graphs of the $\text{CF}_4 \dots \text{Cl}^-$ (left) and $\text{GeF}_4 \dots \text{Cl}^-$ (right) complexes, solid and broken lines correspond to bond paths, big circles to attractors and small green circles to BCPs (red ones—RCPs), the reactive surface ($\nabla^2 \rho(r) = 0$ isosurface) is presented

increases. For example, for the CH_3F , SiH_3F and GeH_3F series the maximum EP at tetrel atom, in the elongation of fluorine—tetrel center bond, is equal to +0.033, +0.062 and +0.068 au, respectively [45]. Hence the $\text{S}_{\text{N}}2$ reaction mentioned earlier here and preceded by the tetrel bond is more probable for the tin species than for the germanium one. There is also the influence of the size effect. It was claimed that the methyl groups are more important to block the tetrel center if the latter one is characterized by the smaller size [60]. Figure 15.15 presents a similar situation of the influence of fluorine substituents for the $\text{CF}_4 \dots \text{Cl}^-$ and $\text{GeF}_4 \dots \text{Cl}^-$ complexes. For the carbon species the Cl-attractor is linked by the bond paths with the fluorine attractors of CF_4 species; in a case of the germanium complex there is the Cl...Ge intermolecular bond path what means that for the germanium complex the $\text{S}_{\text{N}}2$ reaction is more probable.

The similar situation occurs for ammonium cation, NH_4^+ and its analogues, PH_4^+ and AsH_4^+ [50]. However for those cations the whole molecular surfaces are characterized by the positive EP thus they do not act as Lewis bases. For the NH_4^+ ion the maximum EP amounts +0.286 au and it is attributed to the H-atoms while the minimum to the nitrogen center, +0.263 au. This is why for the complexes with hydrogen cyanide (through N-center) as well as with the other Lewis base centers [61], firstly the H-atoms of ammonia cation are involved in interactions and next the links are formed with the nitrogen center of NH_4^+ . For example, for the $\text{NH}_4^+ \dots (\text{NCH})_n$ clusters, the N—H...N hydrogen bonds are formed for $n \leq 4$ and next, when all H-atoms are saturated by the hydrogen bonds the N...N links are created. The latter ones correspond to the σ -hole bonds. Figure 15.16 presents the $\text{NH}_4^+ \dots (\text{NCH})_5$ cluster where one can observe four N—H...N hydrogen bonds and one N...N interaction; for all interactions the corresponding bond paths exist.

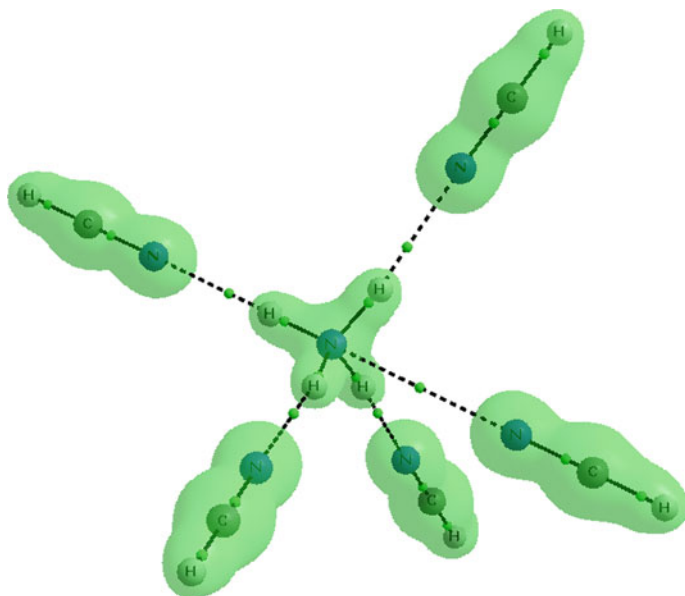


Fig. 15.16 The molecular graph of the $\text{NH}_4^+ \dots (\text{NCH})_5$ complex, solid and broken lines correspond to bond paths, big circles to attractors and small green circles to BCPs, the reactive surface ($\nabla^2 \rho(r) = 0$ isosurface) is presented

15.4 The Case of Hydrogen Bond

It was discussed that the A–H...B hydrogen bond may be classified as a case of the σ -hole bond [33, 62]. For the A–H bond, similarly as for other covalent bonds where the σ -hole is observed, there is the electron charge density shift from H-atom to the A-center. However the mechanism of the σ -hole formation is different for the H-atom than for the other heavier atoms [33, 63]. In a case of pnictogen, chalcogen and halogen atoms p-electron is involved in the σ -bond what results in the depletion of the electron density in outermost part of the center considered and a small area of the increased electrostatic potential, often up to the positive value [26, 27]. Such a region of the positive EP, if exists, is surrounded by areas of the negative EP. There are exceptions, as for example for the tetrel atoms or multivalent halogens described earlier here, where the whole centers are characterized by the positive EP. For the H-atom the whole hemisphere is characterized by the positive EP and there is the single s-type electron involved in the A–H bond, the polarization of this bond results in the additional increase of the EP at the hydrogen atom.

This is interesting that for the protic H-atom in A–H bond there is the detectable shift of its electron density maximum towards the A-center. This effect is not observed for halogen, chalcogen or any others heavier atoms. That may be calculated within the QTAIM approach since the positions of attractors correspond to the

Table 15.1 A–H bonds of selected molecules and cations (A designates heavy atom); r —the distance between A and H attractors; R —the distance between A and H nuclei; $\Delta R\%$ is equal to $[(R-r)/R]*100\%$; ϵ —electronegativity of the A heavy atom in the Pauling scale; distances in Å

Species	r	R	$R-r$	$\Delta R\%$	ϵ
H ₂ O	0.934	0.961	0.027	2.8	3.44
H ₂ S	1.321	1.336	0.015	1.1	2.58
HF	0.888	0.922	0.034	3.7	3.98
HCl	1.256	1.274	0.018	1.4	3.16
NH ₃	0.990	1.012	0.022	2.2	3.04
PH ₃	1.401	1.413	0.012	0.9	2.19
CH ₄	1.070	1.086	0.016	1.5	2.55
SiH ₄	1.467	1.477	0.010	0.7	1.9
H ₃ O ⁺	0.947	0.980	0.032	3.3	3.44
H ₃ S ⁺	1.334	1.351	0.017	1.3	2.58
NH ₄ ⁺	0.997	1.022	0.025	2.5	3.04
PH ₄ ⁺	1.377	1.392	0.015	1.1	2.19

positions of the local maxima of the electron density; they may be attributed to the positions of atoms. However if one assumes that the atoms' positions correspond to nuclei thus this is not the same. Table 15.1 presents MP2/aug-cc-pVTZ results for the selected molecules and cations containing hydrogen atoms. One can see that for all systems considered, for A–H bonds (A = C, N, O, F, Si, P, S, Cl) the distance between the attractors (r) is shorter than the distance between corresponding nuclei (R). Since the positions of attractors and nuclei for heavy (non-hydrogen) atoms are practically the same thus the $R-r$ difference is exactly the shift of the electron density maximum of H-atom from the corresponding nucleus to the A-atom. The $R-r$ difference may be also read as the distance between the nucleus of H-atom and its attractor. The range of those differences is between 0.01 Å and 0.03 Å (Table 15.1), the greatest values are observed for the HF molecule and H₃O⁺ cation, 0.034 Å and 0.032 Å, respectively. The $\Delta R\%$ values relate those differences to the R distances (between nuclei) since $\Delta R\% = [(R-r)/R]100\%$.

It seems that the greatest $R-r$ differences occur for the more electronegative A-atoms; this seems to be natural since the more electronegative center withdraws easier the electron density. Figure 15.17 presents the dependence between the electron charge density shift (expressed as the $\Delta R\%$ value) and the electronegativity of the non-hydrogen A-atom. The results for molecules and cations are included. One can see correlations within the periods, i.e. if the A-atom belongs to the same period and only the neutral species are considered. In a case of cations there is the greater electron charge density shift if one compares it with the neutral molecules. For example, the $R-r$ value for the NH₃ molecule is equal to 0.022 Å while for the NH₄⁺ cation it amounts 0.025 Å; for H₂O and H₃O⁺ species it is equal to 0.027 Å and 0.032 Å, respectively.

Figure 15.18 presents the O–H bond length histograms based on results from Cambridge Structural Database (CSD) [64]; X-ray and neutron diffraction results are presented separately. The CSD searches were performed for all derivatives of benzene containing OH group, this means that not only phenol is considered but

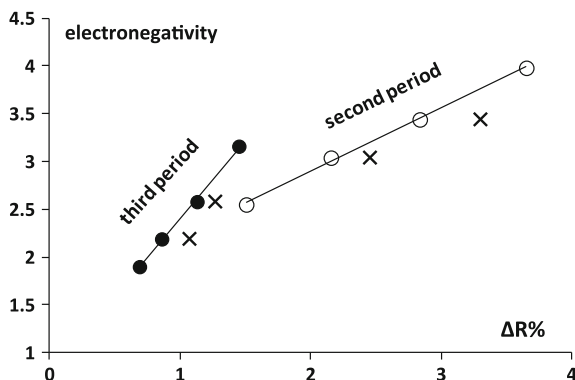


Fig. 15.17 The relationship between $\Delta R\%$ value (for species collected in Table 15.1) and the electronegativity of the A non-hydrogen atom, circles correspond to neutral molecules while crosses to cations

also species where other H-atoms of benzene are substituted. Of course such substituents may influence on the electron density distribution including the hydroxyl group. However the aim of those searches was only to evaluate briefly the differences between the neutron and X-ray diffraction results if the covalent bond containing H-atom is considered. In a case of the neutron diffraction the positions of atoms in the crystal correspond to the positions of nuclei while for the X-ray measurements these are the positions of the local maxima of electron density; in other words in the latter case we have the positions of attractors. This is why the QTAIM approach may be applied for the crystal structures' results [1–3] and for numerous crystal structures the topological analysis based on the experimental electron density is performed. The mentioned above searches on the phenol derivatives were carried out for high quality measurements since the following search criteria were applied: no disordered structures, no structures with unresolved errors, no powder structures, no polymeric structures, e.s.d.'s for C–C bonds $\leq 0.005 \text{ \AA}$ and the discrepancy index $R \leq 7 \%$.

The precision of the determination of the positions of the maxima of electron density for H-atoms in X-ray diffraction measurements is much lower than the precision of determination of hydrogen nuclei positions in the neutron diffraction [8] but one can see that statistically the X-ray O–H bonds are much shorter than the neutron diffraction counterparts (Fig. 15.18); the mean OH bond length for X-ray experiments is equal to 0.871 \AA while this value for neutron diffraction amounts 0.990 \AA ; the corresponding median values are equal to 0.841 \AA and 0.984 \AA , respectively. The median values are presented here since the bond length distributions are not the normal ones. The number of the OH bonds included in the histograms (Fig. 15.18) for the X-ray and neutron diffraction is equal to 3798 and 12, respectively. This is because, in general, the number of X-ray observations collected in CSD is large in comparison with the neutron diffraction ones; the total number of crystal structures stored into Cambridge Structural Database is equal to

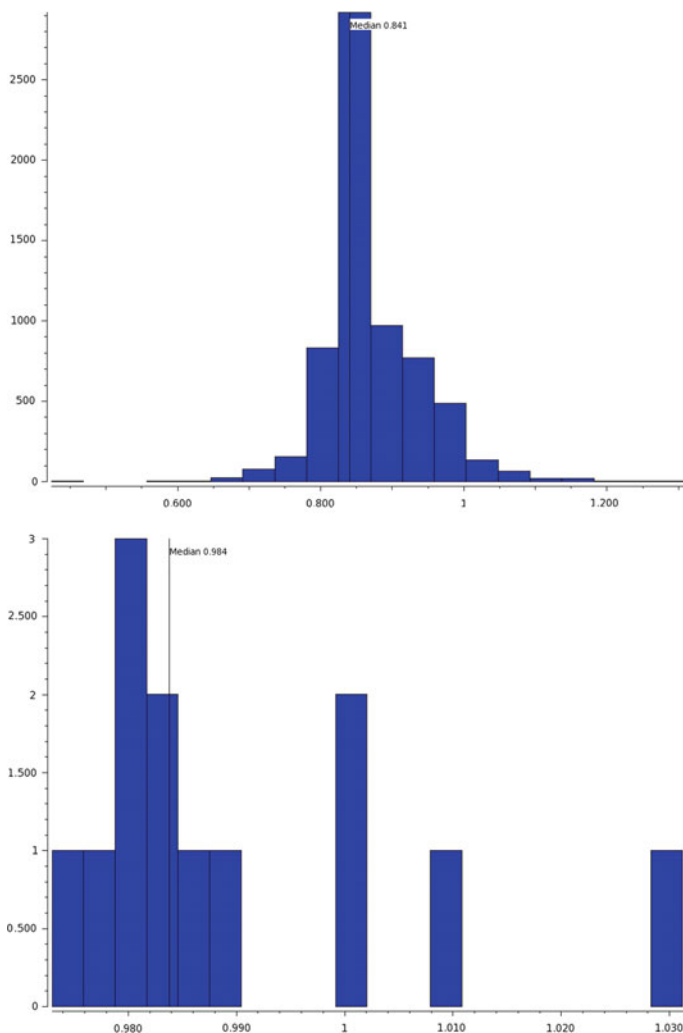


Fig. 15.18 Histograms of the O-H bond length for O-H groups connected with benzene ring detected in crystal structures, neutron diffraction (*down*) and X-ray diffraction results (*up*) are presented. The *horizontal* axes correspond to O-H bonds (length in Å), the *vertical* axes to number of observations, based on the results from the Cambridge Structural Database [64]

686 944 while only 1616 of them are the neutron diffraction measurements (CSD summary statistics—6 January 2014 [65]). It is worth mentioning that the total number of crystal structures deposited in CSD at the end of 2014 reached 750 200. In spite of the great disproportion between the number of neutron diffraction and X-ray results one can see that the experimental results clearly show that there is the electron charge density shift from H-atom to the bonded center, in the case considered here (Fig. 15.18) to the oxygen atom.

In view of those results one may say that the positive EP at hydrogen atom is enhanced owing to the electron density shift and that the links of H-atom with Lewis base centers, i.e. hydrogen bonds, may be classified as the σ -hole bonds. An example of the complex connected through two hydrogen bonds, O–H...F and C–H...O, was considered in the introduction (see Fig. 15.1). These are the classical examples of 3c-4e (3 center—4 electron) A–H...B hydrogen bonds since there are A, H and B centers, 2 electrons of the A–H σ -bond and the lone electron pair of the proton acceptor (B). However the A–H... π interactions, where it is difficult to indicate the single B-center, are also classified as hydrogen bonds. It is commonly accepted that for those interactions π -electrons play the role of the Lewis base.

Figure 15.19 shows the molecular graphs of the $C_2H_2...HF$ T-shaped complex; two graphs with the isolines of the laplacian of electron density corresponding to two levels of calculations (MP2/aug-cc-pVTZ and MP2/aug-cc-pVQZ) are presented. In both cases there is the bond path linking the H-atom attractor of HF molecule with the π -electron system of acetylene; in the case of aug-cc-pVTZ basis set there is the link between H-attractor and the non-nuclear attractor (NNA) situated between carbon atoms, in a case of the aug-cc-pVQZ basis set there is the hydrogen-bond critical point (H...BCP) link. Practically there is no the significant difference between those results, one may say that both NNA and BCP mimic the one-center π -electron Lewis base. This is worth to mention that such H... π bond paths for hydrogen bonded systems were analyzed before [66]. The characteristics of the BCP corresponding to the H... π bond path are practically the same for both levels (ρ_{BCP} and $\nabla^2\rho_{BCP}$ are equal to 0.021 au and 0.049 au,

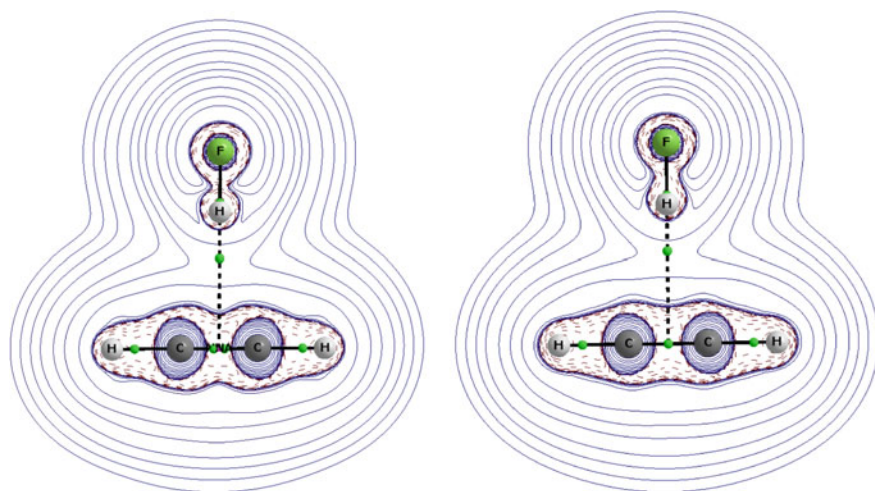


Fig. 15.19 The molecular graphs of the $C_2H_2...HF$ complex, the MP2/aug-cc-pVTZ (left) and MP2/aug-cc-pVQZ (right) levels, solid and broken lines correspond to bond paths, big circles to attractors and small green circles to BCPs, the isolines of Laplacian of electron density are also presented; there is non-nuclear attractor (small red circle) between carbon atoms (left) for the MP2/aug-cc-pVTZ level

respectively; the remaining characteristics differ only slightly). The characteristics of BCP situated between carbon atoms for the aug-cc-pVQZ basis set are as follows; $\rho_{\text{BCP}} = 0.416$ au and $\nabla^2\rho_{\text{BCP}} = -1.274$ au while for the aug-cc-pVTZ basis set there are two BCPs between carbon attractors for which $\rho_{\text{BCP}} = 0.411$ au and $\nabla^2\rho_{\text{BCP}} = -1.278$ au, there is also NNA situated between latter BCPs where $\rho_{\text{BCP}} = 0.411$ au and $\nabla^2\rho_{\text{BCP}} = -1.370$ au.

The situation is more complicated if the multicenter (more than 2 centers) π -electron system plays the role of proton acceptor in hydrogen bond interaction. It is often stated in the literature that aromatic systems or other closed-ring π -electron systems may play the role of proton acceptors in hydrogen bonds [67]; such species as benzene, antracene, cyclopentadienyl anion and their derivatives as well as other moieties are often considered. This means that π -electrons as a whole are treated as the Lewis base center. The hydrogen bonds with the multicenter π -electron systems were analyzed recently (the calculations were performed at the MP2/6-311 ++G(d, p) level) and it was found that at least few sub-classes of the A–H... π hydrogen bonds may be considered [68]. Figure 15.20 presents the molecular graphs of the $\text{C}_6\text{H}_6\text{...HCCH}$, $\text{C}_6\text{H}_6\text{...HF}$ and $\text{C}_5\text{H}_5^-\text{...HF}$ complexes. The binding energy for the $\text{C}_6\text{H}_6\text{...HCCH}$ complex amounts -2.1 kcal/mol (BSSE correction included), the complex is characterized by the C_{6v} symmetry and the molecular graph (Fig. 15.20) reflects this symmetry since six H...C bond paths between the hydrogen of acetylene and the carbon attractors of benzene are observed. For the BCPs of those bond paths the following characteristics were found; $\rho_{\text{BCP}} = 0.007$ au and $\nabla^2\rho_{\text{BCP}} = 0.023$ au. One may say that the C–H... π hydrogen bond is classified here as rather weak interaction and that all C-atoms of the benzene ring are involved equivalently in that interaction. On the other hand one may say that there are six equivalent C–H...C interactions for the $\text{C}_6\text{H}_6\text{...HCCH}$ complex (bifurcated hydrogen bond); this situation is different than for the $\text{C}_2\text{H}_2\text{...HF}$ complex presented earlier here where the H...BCP (or H...NNA) bond path was observed and where

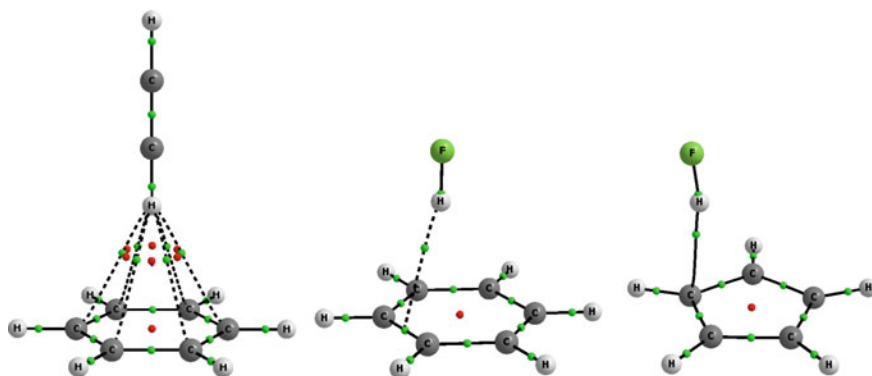


Fig. 15.20 The molecular graphs of the $\text{C}_6\text{H}_6\text{...HCCH}$, $\text{C}_6\text{H}_6\text{...HF}$ and $\text{C}_5\text{H}_5^-\text{...HF}$ complexes (from left to right), the MP2/6-311 ++G(d,p) level, solid and broken lines correspond to bond paths, big circles to attractors and small circles to critical points (green—BCPs, red—RCPs)

the BCP (or NNA) of the triple $C \equiv C$ bond mimics the one-center Lewis base. Since within the NBO approach the Lewis type structures are considered thus three $\pi_{CC} \rightarrow \sigma_{CH}^*$ intermolecular orbital-orbital interactions were found here, each of the energy amounting 0.4 kcal/mol and each corresponding to the overlap of CC π -bond orbital of benzene and the antibonding CH orbital of acetylene. The high C_{6v} structure symmetry results in the same electron charge distribution symmetry thus as it was pointed out earlier here, there are six equivalent C...H bond paths between acetylene and benzene as well as the equivalent charges for benzene atoms are detected (NBO charges for C and H atoms are equal to -0.208 au and $+0.209$ au, respectively; the corresponding charges for isolated benzene are equal to -0.204 au and $+0.204$ au).

For the $C_6H_6 \dots HF$ complex there is the H...BCP bond path between the HF molecule and the BCP of the CC bond of benzene; thus it is the similar situation to that one occurring for the $C_2H_2 \dots HF$ complex. The interaction is stronger here than for the complex of benzene with acetylene since the binding energy is equal to -3.3 kcal/mol; the following characteristics were found for the BCP of the mentioned above H...BCP bond path; $\rho_{BCP} = 0.010$ au and $\nabla^2 \rho_{BCP} = 0.031$ au. One can see that the C_{6v} symmetry is broken here; two carbon atoms are distinguished since the BCP of the path between them mimics the one-center Lewis base for this complex. The charges of those carbon atoms in the C_6H_6-HF complex are the most negative ones since they are equal to -0.225 au while the remaining C-charges amount -0.204 au; besides the intermolecular H...C distances are smallest for these carbons, 2.503 Å, while the remaining H...C (HF-benzene) distances amount $2.724-2.929$ Å. This means that the bond path between HF and C_6H_6 molecules shows the preferable H...C interactions. What is the reason of such an orientation of the HF molecule in the C_6H_6-HF complex? Probably for this structure the electrostatic interactions between benzene and HF are more attractive than in a case of the C_{6v} symmetry complex. However the difference is not significant; the MP2/aug-cc-pVTZ calculations show that the transition state C_{6v} symmetry C_6H_6-HF complex is higher in energy than the corresponding complex being in the energetic minimum only by 0.1 kcal/mol. The single $\pi_{CC} \rightarrow \sigma_{CH}^*$ orbital-orbital interaction is observed for the C_6H_6-HF complex with the interaction energy of 1.1 kcal/mol; the CC bond π -orbital corresponds here to the CC BCP which is connected with the H-atom attractor of HF molecule (see Fig. 15.20).

Figure 15.20 presents also the $C_5H_5^- \dots HF$ complex where the F-H... π hydrogen bond is assisted by the negative charge. It results in the stronger $C_5H_5^- - HF$ interaction since the binding energy is equal to -16.3 kcal/mol. The molecular graph shows the single H...C bond path where the following characteristic of the corresponding BCP were calculated; $\rho_{BCP} = 0.028$ au and $\nabla^2 \rho_{BCP} = 0.056$ au. The total electron energy density, H_{BCP} , at this bond critical point is equal to -0.002 au what may be explained by the partly covalent in nature corresponding H...C interaction. Also in this case, similarly as it was found for the C_6H_6-HF complex, the bond path shows the preferable H...C interaction since the charge of the corresponding C-atom of the $C_5H_5^-$ anion is equal to -0.433 au while for the remaining carbons of the anion this charge is situated in a range between -0.350 au

and -0.353 au. The H...C distance corresponding to the bond path is equal to 2.007 Å while the remaining distances amount 2.395 – 2.902 Å. This is worth to mention that for the $C_5H_5^- \dots HF$ complex a lone electron pair orbital within the NBO approach is detected for the carbon atom of $C_5H_5^-$ and that this orbital is involved in the most important $n(C) \rightarrow \sigma_{CH}^*$ orbital-orbital overlap for which the energy of interaction amounts 9.7 kcal/mol; this orbital is located at the C-atom connected by the bond path with HF molecule.

One can see that for the A–H... π hydrogen bonds presented here there are significant structural differences between them; those differences are reflected in the geometry as well as in the electron charge distributions. One can observe hydrogen bonds where the protic H-atom is linked with the Lewis base by atom-atom bond path (in $C_5H_5^- \dots HF$), by the atom-BCP bond path (in $C_6H_6 \dots HF$ or $C_2H_2 \dots HF$) and by the few equivalent atom-atom bond paths (in the $C_6H_6 \dots HCCH$ complex). In such a situation the question arises if the meaning of the term A–H... π hydrogen bonds should be revised. For example, maybe for the $C_5H_5^- \dots HF$ complex the term F–H...C hydrogen bond is more proper than the F–H... π one and maybe for the $C_6H_6 \dots HCCH$ complex the bifurcated hydrogen bond (six F–H...C intermolecular contacts) should be applied.

It is interesting that also σ -electrons may play a role of the proton acceptor in the hydrogen bonds; they are designated as the A–H... σ interactions. Such systems were analyzed theoretically for the $FH \dots H_2$, $H_3O^+ \dots H_2$, $NH_4^+ \dots H_2$ and other complexes where the molecular hydrogen acts as the Lewis base [69–72]. For all of them the situation is similar to that one occurring for the $C_2H_2 \dots HF$ complex; i.e. there is the bond path linking the hydrogen protic atom of the Lewis acid unit with the bond critical point of H–H molecular hydrogen bond. Figure 15.21 presents the molecular graph of the $NH_4^+ \dots H_2$ complex where one may observe this type of the bond path. One can see that for this complex the N–H bond of ammonia cation is located perpendicularly (or nearly so) to the H_2 molecule. Such T-shaped structures are observed for other complexes mentioned here, where the σ -electrons of the molecular hydrogen are the proton acceptor in hydrogen bonds [71]. For the $NH_4^+ \dots H_2$ complex the binding energy is equal to -2.3 kcal/mol (MP2/6-311 ++ (3df,3pd) level, BSSE included), the ρ_{BCP} and $\nabla^2\rho_{BCP}$ values for the BCP corresponding to the H...BCP bond path linking ammonia cation with H_2 molecule are equal to 0.013 au and 0.041 au, respectively. This is interesting that the most important orbital-orbital interaction corresponds here to the $\sigma_{H-H} \rightarrow \sigma_{N-H}^*$ overlap where σ_{H-H} is the σ -bond orbital of molecular hydrogen while σ_{N-H}^* is the anti-bonding N–H orbital of ammonia cation, the corresponding energy of interaction is equal to 3.6 kcal/mol (HF/6-311 ++G(d,p)//MP2/6-311 ++G(d,p) level).

The existence of the A–H... σ hydrogen bonds was confirmed by experiment. For example, gas phase measurements of dipole moment and vibrational predissociation lifetimes as well as the determination of rotational constants performed for the F–H... H_2 complex [73] confirmed its T-shaped structure. The high-resolution infrared spectra were analyzed for the H_2 –HF, D_2 –HF and HD–HF complexes solvated in helium nanodroplets and also for those species the T-shaped structure was confirmed [74–76]. The infrared vibrational predissociation spectra

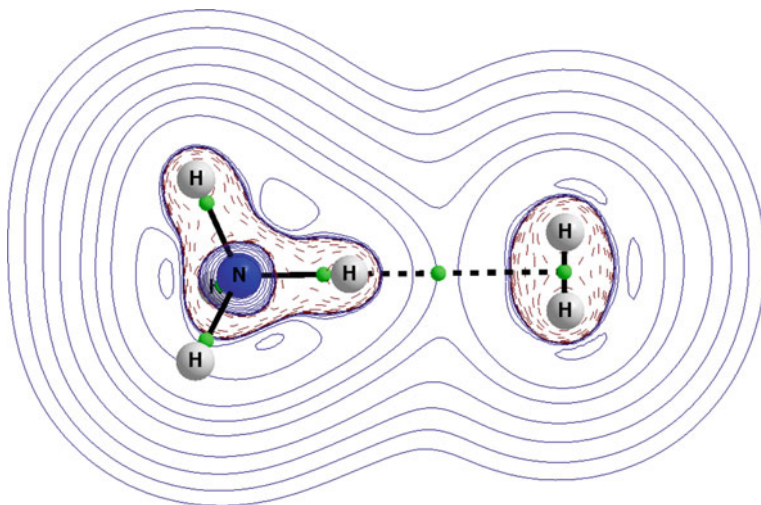


Fig. 15.21 The molecular graph of the $\text{NH}_4^+ \dots \text{H}_2$ complex, solid and broken lines correspond to bond paths, big circles to attractors and small green circles to BCPs, the isolines of Laplacian of electron density are presented; the projection in the plane containing H_2 molecule and HNH atoms of NH_4^+ cation

measurements were carried out for the $\text{H}_2\text{-HCO}^+$ complex linked through $\text{C-H} \dots \sigma$ interaction, where the σ -electrons of the molecular hydrogen act as the Lewis base [77]. The authors did not consider the $\text{C-H} \dots \sigma$ interaction as the hydrogen bond; however the results of experiment clearly show that this arrangement possesses characteristics typical for the latter kind of interaction.

Finally it is worth mentioning that the clusters of ammonia cation, NH_4^+ , with H_2 molecules— $(\text{NH}_4^+)(\text{H}_2)_n$ (n up to 8) were calculated [69, 78]. It was also found that the whole molecular surface of ammonia cation (0.001 au electron density surface was considered) is characterized by the positive EP; however the EP maxima are attributed to H-atoms [50]. Hence the increase of the number of molecular hydrogen molecules surrounding ammonia cation results in the $\text{N-H} \dots \sigma$ hydrogen bonds formation and when all N-H bonds are saturated by those interactions (for $n = 4$) thus next H_2 molecules (for clusters with $n \geq 5$) are linked with the nitrogen center of the cation, however all H_2 molecules for those clusters act as Lewis bases through their σ -electrons. The situation is very similar to that one occurring for the $(\text{NH}_4^+)(\text{HCN})_n$ clusters [61] mentioned earlier here (see also Fig. 15.16).

This is interesting that the molecular hydrogen possesses the properties of Lewis base (σ -electrons) and of the Lewis acid what is reflected in the distribution of electrostatic potential which is negative along the H-H σ -bond and it is positive at the outermost parts of H-atoms [79]. One may expect that the interaction of the H_2 molecule with Lewis acids should result in its connection through H-H BCP while the interaction with Lewis bases should result in the connection of the H_2 species by

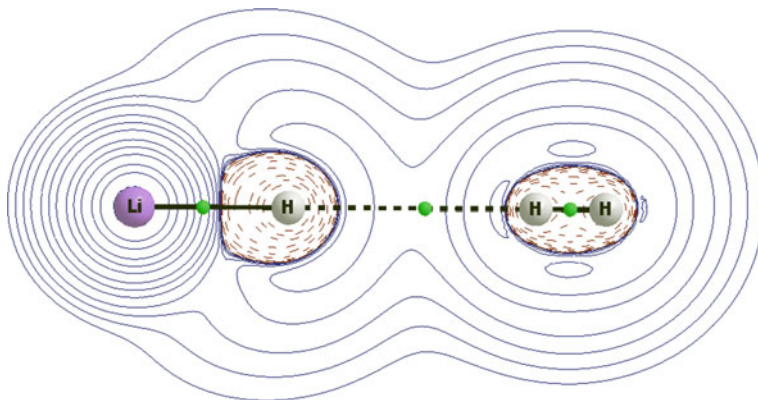


Fig. 15.22 The molecular graph of the LiH...H₂ complex, solid and broken lines correspond to bond paths, big circles to attractors and small green circles to BCPs, the isolines of Laplacian of electron density are also presented

one of its H-attractors. Figure 15.22 presents the latter situation where H₂ interacts as the Lewis acid with the hydride Lewis base center of LiH species. Figure 15.22 clearly shows the H...H bond path linking basic (of LiH) and acidic (of H₂) hydrogen atoms. This kind of interaction is known as the dihydrogen bond [80–83] and really, early on the LiH...H–H system was classified as linked by this type of interaction [84].

The distribution of the laplacian of electron density (Fig. 15.22) shows the vertical to the H–H σ -bond concentration of the electron density and this density depletion at the edges of H-atoms of hydrogen molecule. There is a very interesting distribution for the LiH species where it is clear that hydride anion interacts with the electron density deprived Li cation. The most important orbital-orbital interaction corresponds here to the $\sigma_{\text{Li-H}}^* \rightarrow \sigma_{\text{H-H}}^*$ overlap where $\sigma_{\text{Li-H}}$ is the σ -bond orbital of LiH molecule while $\sigma_{\text{H-H}}^*$ is the antibonding H–H orbital of dihydrogen, the corresponding energy of interaction is equal to 1.7 kcal/mol. The polarization of the H₂ molecule is observed here since the NBO atomic charges are equal to +0.031 au and –0.036 au (the positively charged H-atom is in contact with the negatively charged H-atom of the LiH species). One can see that the whole H₂ molecule is slightly negatively charged, this is because of the acidic properties of H₂ in this complex what results in the electron density shift from the LiH species to the dihydrogen. This is worth mentioning that such polarization does not occur for the dihydrogen in the NH₄⁺...H₂ complex considered earlier here since atomic charges of H-atoms in the dihydrogen are both equal to +0.007 au. In the latter complex the H₂ molecule is slightly positively charged since there is outflow of the electron density from that species due to its Lewis base characteristics.

The analysis of interactions of dihydrogen with other species seems to be very important to understand the mechanisms of numerous reactions and processes such as for example, the activation of molecular hydrogen and next its splitting at

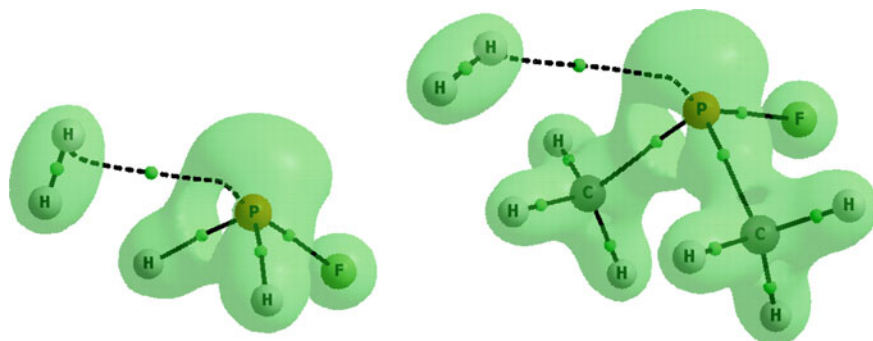


Fig. 15.23 The molecular graphs of the $\text{PFH}_2\dots\text{H}_2$ (left) and $\text{PF}(\text{CH}_3)_2\dots\text{H}_2$ (right) complexes, solid and broken lines correspond to bond paths, big circles to attractors and small green circles to BCPs, the reactive surface ($\nabla^2\rho(r) = 0$ isosurface) is presented

reaction center [85]; usually the metallic center is considered both experimentally [86] and theoretically [87].

Figure 15.23 presents molecular graphs of two complexes where dihydrogen interacts with the phosphorus (non-metallic) center, i.e. the $\text{PFH}_2\dots\text{H}_2$ and $\text{PF}(\text{CH}_3)_2\dots\text{H}_2$ complexes are considered. In both cases the P-center is characterized by the Lewis acid properties due to the existence of the σ -hole since the regions of the positive EP situated in the elongation of F–P bond are observed. The σ -holes located at the P-centers are characterized by the positive EPs which amount 0.060 au and 0.037 au for the PFH_2 and $\text{PF}(\text{CH}_3)_2$ monomers, respectively. The binding energies for the $\text{PFH}_2\text{--H}_2$ and $\text{PF}(\text{CH}_3)_2\text{--H}_2$ systems are equal to -1.2 kcal/mol and -0.7 kcal/mol, respectively (not corrected for BSSE).

There is an interesting issue if the dihydrogen in those complexes reveals its Lewis acid or Lewis base properties. Figure 15.23 shows that for the $\text{PFH}_2\text{--H}_2$ complex the P–dihydrogen intermolecular bond path crosses the region of the σ -hole but very close to the region of the electron charge concentration corresponding to the unshared P electron pair and next this bond path is aimed to the BCP of dihydrogen; however finally it ends at the H-atom attractor. The non-linear trajectory of the bond path does not show ambiguously the nature of centers being in contact; one may rather expect that the dihydrogen interacts as the Lewis base with the Lewis acid region of phosphorus. Two most important orbital-orbital interactions are detected for this complex; $\sigma(\text{H}_2) \rightarrow \sigma^*(\text{P--F})$ and $n(\text{P}) \rightarrow \sigma^*(\text{H}_2)$ which correspond to the Lewis base and Lewis acid properties of dihydrogen, respectively. The energy of interaction for the former overlap is equal to 1.5 kcal/mol while it amounts 0.6 kcal/mol for the latter overlap. Thus according to the NBO approach, the dihydrogen reveals stronger Lewis base properties than the Lewis acid ones in the $\text{PFH}_2\dots\text{H}_2$ complex.

The different picture is observed for the $\text{PF}(\text{CH}_3)_2\text{--H}_2$ complex where the trajectory of the P...dihydrogen bond path prompts the Lewis acid properties of H_2 and Lewis base properties of the phosphorus species since the bond path crosses the

lone electron pair region of P-center and it clearly ends at one of H-atoms of the dihydrogen. The NBO results confirm that since the $\sigma(\text{H}_2) \rightarrow \sigma^*(\text{P-F})$ and $n(\text{P}) \rightarrow \sigma^*(\text{H}_2)$ orbital-orbital energies of interactions are equal to 0.2 kcal/mol and 0.6 kcal/mol, respectively showing the stronger Lewis acid properties of the dihydrogen in that complex.

The interactions of molecular hydrogen with the $\text{PF}(\text{CH}_3)_2$ and PFH_2 species are classified as weak ones thus there are only slight electron density shifts for the corresponding complexes, -0.002 au and +0.008 au for the $\text{PFH}_2\text{-H}_2$ and $\text{PF}(\text{CH}_3)_2\text{-H}_2$ complexes, respectively (NBO results). This means that for the $\text{PFH}_2\text{-H}_2$ complex there is the shift from the H_2 molecule while for the $\text{PF}(\text{CH}_3)_2\text{-H}_2$ complex the shift to the dihydrogen is observed. Those shifts clearly confirm the results presented earlier here of the Lewis base or Lewis acid properties of the molecular hydrogen.

15.5 Summary

The analysis of the location of bond paths, of their trajectories and the distribution of the electron density in species analyzed, especially if such a distribution is discussed on the basis of the laplacian of the electron density, are very useful tools to deepen the understanding of the nature of interactions. This is also important that the analysis of the molecular graphs is often in line with the results of other approaches. This is worth mentioning that the molecular graph may be treated as a source of information on the location of atomic attractors (positions of atoms) and on the location of bond paths corresponding to the preferable stabilizing interactions.

Let us look at examples presented in this chapter; it is evident, that very often for weak interactions the atom-atom contacts correspond to Lewis acid-Lewis base centers' contacts characterized by the opposite electrostatic potentials. The hydrogen bonded systems are examples of such a situation, or even more generally, the σ -hole bonds. This is interesting that the bond paths, for weak interactions, usually connect the local maximum of EP with the minimum of EP. The complexes of the BrF_5 characterized by the pentavalent bromine center are examples of that situation; there are four equivalent local maxima of EP at the Br center situated symmetrically around the fourfold axis of symmetry of the BrF_5 molecule. This is why the complexes of BrF_5 with weak Lewis bases are not linear since the bond path crosses one of the local maxima of bromine. However the interactions with stronger Lewis bases like F^- or Cl^- anions lead to the meaningful changes in the electron charge distribution what results in the formation of BrF_6^- and BrF_5Cl^- complexes with the $\text{F-Br}\dots\text{F}^-$ and $\text{F-Br}\dots\text{Cl}^-$ linear arrangements, respectively.

One can enumerate other examples where the molecular graphs inform of the kinds and of the nature of interactions. The complexes of molecular hydrogen may be mentioned here. The dihydrogen possesses Lewis acid and Lewis base characteristics since the positive electrostatic potential is observed at the H-atoms, at edges

of the H–H bond while the negative EP is connected with the σ -bond. This is why the H₂ molecule interacts with Lewis acid centers through its σ -electrons and in the corresponding molecular graphs the bond paths between the Lewis acid center and the bond critical point of the H–H σ -bond are observed. On the other hand if the H₂ molecule reveals their Lewis acid properties thus the bond paths between H-atom of molecular hydrogen and the Lewis base center may be observed.

In general the contour maps of the laplacian of the electron density nicely show the links between the regions of the electron density depletion with the regions of its concentration; this was rationalized recently by Eskandari and coworkers in terms of the lump-hole interactions concept [55, 56].

Acknowledgments Financial support comes from Eusko Jaurlaritza (GIC 07/85 IT-330-07) and the Spanish Office for Scientific Research (CTQ2011-27374). Technical and human support provided by Informatikako Zerbitzu Orokorra - Servicio General de Informatica de la Universidad del Pais Vasco (SGI/IZO-SGIker UPV/EHU), Ministerio de Ciencia e Innovación (MICINN), Gobierno Vasco Eusko Jaurlaritza (GV/EJ), European Social Fund (ESF) is gratefully acknowledged. The QTAIM calculations as well as the corresponding figures were performed with the use of the AIMAll program [88].

References

1. Tsirelson VG, Ozerov RP (1996) Electron density and bonding in crystals. Institute of Physics, Bristol, Philadelphia
2. Coppens P (1997) X-Ray charge densities and chemical bonding. Oxford University Press, IUCr
3. Koritszansky TS, Coppens P (2001) Chemical applications of X-ray charge density analysis. Chem Rev 101:1583–1638
4. Bader RFW (1985) Atoms in molecules. Acc Chem Res 18:9–15
5. Bader RFW (1990) Atoms in molecules, a quantum theory. Oxford University Press, Oxford
6. Popelier P (2000) Atoms in molecules. an introduction. Prentice Hall, Pearson Education Limited, Harlow
7. Matta C, Boyd RJ (ed) (2007) Quantum theory of atoms in molecules: recent progress in theory and application. Wiley-VCH
8. Dunitz JD (1979) X-Ray analysis and the structure of organic molecules. Cornell University Press, Ithaca, p 395
9. Bader RFW (1998) A bond path: a universal indicator of bonded interactions. J Phys Chem A 102:7314–7323
10. Bader RFW (2009) Bond paths are not chemical bonds. J Phys Chem A 113:10391–10396
11. Runtz GR, Bader RFW, Messer RR (1977) Definition of bond paths and bond directions in terms of the molecular charge distribution. Can J Chem 55:3040–3045
12. Keith TA, Bader RFW, Aray Y (1996) Structural homeomorphism between the electron density and the virial field. Int J Quantum Chem 57:183–198
13. Gatti C, Cargnoni F, Bertini L (2003) Chemical information from the source function. J Comput Chem 24:422–436
14. Gatti C (2005) Chemical bonding in crystals: new directions. Z Kristallogr 220:399–457
15. Stalke D (2011) Meaningful structural descriptors from charge density. Chem Eur J 17:9264–9278

16. Rozas I, Alkorta I, Elguero J (2000) Behavior of ylides containing N, O, and C atoms as hydrogen bond acceptors. *J Am Chem Soc* 122:1154–11161
17. Grabowski SJ (2011) What is the covalency of hydrogen bonding? *Chem Rev* 11:2597–2625
18. Cremer D, Kraka E (1984) A description of the chemical-bond in terms of local properties of electrodensity and energy. *Croat Chem Acta* 57:1259–1281
19. Jenkins S, Morrison I (2000) The chemical character of the intermolecular bonds of seven phases of ice as revealed by ab initio calculation of electron densities. *Chem Phys Lett* 317:97–102
20. Grabowski SJ (2001) Ab initio calculations on conventional and unconventional hydrogen bonds—study of the hydrogen bond strength. *J Phys Chem A* 105:10739–10746
21. Weinhold F, Landis C (2005) Valency and bonding, a natural bond orbital donor—acceptor perspective. Cambridge University Press
22. Reed AE, Curtiss LA, Weinhold F (1988) Intermolecular Interactions from a natural bond orbital, donor-acceptor viewpoint. *Chem Rev* 88:899–926
23. Alabugin IV, Manoharan M, Peabody S, Weinhold F (2003) Electronic basis of improper hydrogen bonding: a subtle balance of hyperconjugation and rehybridization. *J Am Chem Soc* 125:5973–5987
24. Weinhold F, Klein R (2012) What is a hydrogen bond? mutually consistent theoretical and experimental criteria for characterizing H-bonding interactions. *Mol Phys* 110:565–579
25. Murray JS, Lane P, Politzer P (2009) Expansion of the σ -hole concept. *J Mol Model* 15:723–729
26. Politzer P, Murray JS, Clark T (2010) Halogen bonding: an electrostatically-driven highly directional noncovalent interaction. *Phys Chem Chem Phys* 12:7748–7758
27. Politzer P, Murray JS, Clark T (2013) Halogen bonding and other σ -hole interactions: a perspective. *Phys Chem Chem Phys* 15:11178–11189
28. Boys SF, Bernardi F (1970) The calculation of small molecular interactions by the differences of separate total energies. Some procedures with reduced errors. *Mol Phys* 19:553–566
29. Nyburg SC, Faerman CH (1985) A revision of van der Waals atomic radii for molecular crystals: nitrogen, oxygen, fluorine, sulfur, chlorine, selenium, bromine, and iodine bonded to carbon. *Acta Crystallogr B* 41:274–279
30. Zordan F, Brammer L, Sherwood P (2005) Supramolecular chemistry of halogens: complementary features of inorganic (M-X) and organic (C-X') halogens applied to M-X... X'-C halogen bond formations. *J Am Chem Soc* 127:5979–5989
31. Formigué M, Batail P (2004) Activation of hydrogen- and halogen-bonding interactions in tetrathiafulvalene-based crystalline molecular conductors. *Chem Rev* 104:5379–5418
32. Clark T, Hennemann M, Murray JS, Politzer P (2007) Halogen bonding: the σ -hole. *J Mol Model* 13:291–296
33. Clark T (2013) σ -Holes. *Wires Comput Mol Sci* 3:13–20
34. Politzer P, Murray JS, Concha MC (2007) Halogen bonding and the design of new materials: organic bromides, chlorides and perhaps even fluorides as donors. *J Mol Model* 13:643–650
35. Landrum GA, Goldberg N, Hoffmann R, Minyaev RM (1998) Intermolecular interactions between hypervalent molecules: Ph2IX and XF3 (X = Cl, Br, I) dimers. *New J Chem* 22:883–890
36. Wang W (2011) Halogen bond involving hypervalent halogen: CSD search and theoretical study. *J Phys Chem A* 115:9294–9299
37. Grabowski SJ (2014) Halogen bond with the multivalent halogen acting as the Lewis acid center. *Chem Phys Lett* 605–606:131–136
38. Weinhold F, Landis C (2005) Valency and bonding, a natural bond orbital donor—acceptor perspective. Cambridge University Press, pp 275–306
39. Pimentel GC (1951) The bonding of trihalide and bifluoride ions by the molecular-orbital method. *J Chem Phys* 19:446–448
40. Rundle RE (1947) Electron deficient compounds. *J Am Chem Soc* 69:1327–1331
41. Politzer P, Murray JS (2013) Halogen bonding: an interim discussion. *ChemPhysChem* 14:2145–2151

42. Bundhun A, Ramasami P, Murray JS, Politzer P (2012) Trends in σ -hole strengths and interactions of F3MX molecules (M = C, Si, Ge and X = F, Cl, Br, I). *J Mol Mod* 19:2739–2746
43. Bauzá A, Mooibroek TJ, Frontera A (2013) Tetrel-bonding interaction rediscovered supramolecular force? *Angew Chem Int Ed Engl* 52:12317–12321
44. Mani D, Arunan E (2013) The X-C...Y (X = O/F, Y = O/S/F/Cl/Br/N/P) ‘carbon bond’ and hydrophobic interactions. *Phys Chem Chem Phys* 15:14377–14383
45. Grabowski SJ (2014) Tetrel bond— σ -hole bond as a preliminary stage of the S_N2 reaction. *Phys Chem Chem Phys* 16:1824–1834
46. Sundberg MR, Uggla R, Viñas C, Teixidor F, Paavola S, Kivekäs R (2007) Nature of intramolecular interactions in hypercoordinate C-substituted 1,2-dicarba-*closo*-dodecaboranes with short P...P distances. *Inorg Chem Commun* 10:713–716
47. Bauer S, Tschirschwitz S, Lönnecke P, Franck R, Kirchner B, Clark ML, Hey-Hawkins E (2009) Enantiomerically Pure Bis(phosphanyl)carbaborane(12) Compounds. *Eur J Inorg Chem* 2776–2788
48. Del Bene JE, Alkorta I, Sanchez-Sanz G, Elguero J (2011) Structures, energies, bonding, and NMR properties of pnictogen complexes $H_2XP:NXH_2$ (X = H, CH_3 , NH_2 , OH, F, Cl). *J Phys Chem A* 115:13724–13731
49. Scheiner S (2011) Can two trivalent N atoms engage in a direct N...N noncovalent interaction? *Chem Phys Lett* 514:32–35
50. Grabowski SJ (2013) σ -Hole bond versus hydrogen bond: from tetravalent to pentavalent N, P, and as atoms. *Chem Eur J* 19:14600–14611
51. Sanz P, Yañez M, Mó O (2002) Competition between X...H...Y intramolecular hydrogen bonds and X...Y (X = O, S, and Y = Se, Te) chalcogen-chalcogen interactions. *J Phys Chem A* 106:4661–4668
52. Wang W, Ji B, Zhang Y (2009) Chalcogen bond: a sister noncovalent bond to halogen bond. *J Phys Chem A* 113:8132–8135
53. Alikhani E, Fuster F, Madebene B, Grabowski SJ (2014) Topological reaction sites—very strong chalcogen bonds. *Phys Chem Chem Phys* 16:2430–2442
54. Del Bene JE, Alkorta I, Sánchez-Sanz G, Elguero J (2011) ^{31}P - ^{31}P Spin-Spin coupling constants for pnictogen homodimers. *Chem Phys Lett* 512:184–187
55. Del Bene JE, Alkorta I, Elguero J (2015) Substituent effects on the properties of pnictogen-bonded complexes $H_2XP:PYH_2$, for X, Y = F, Cl, OH, NC, CCH, CH_3 , CN, and H. *J Phys Chem A* 119:224–233
56. Eskandari K, Mahmoodabadi N (2013) Pnictogen bonds: a theoretical study based on the laplacian of electron density. *J Phys Chem A* 117:13018–13024
57. Eskandari K, Zariny H (2010) Halogen bonding: a lump-hole interaction. *Chem Phys Lett* 492:9–13
58. Bento AP, Solà M, Bickelhaupt FM (2005) *Ab initio* and DFT benchmark study for nucleophilic substitution at carbon ($S_N2@C$) and silicon ($S_N2@Si$). *J Comput Chem* 26:1497–1504
59. Pierrefixe SCAH, Guerra CF, Bickelhaupt FM (2008) Hypervalent silicon versus carbon: ball-in-a-box model. *Chem Eur J* 14:819–828
60. Levy CJ, Puddephatt RJ (1997) Rapid reversible oxidative addition of group 14-halide bonds to platinum(ii): rates, equilibria, and bond energies. *J Am Chem Soc* 119:10127–10136
61. Grabowski SJ (2014) Clusters of ammonium cation–hydrogen bond versus σ -hole bond. *ChemPhysChem* 15:876–884
62. Murray JS, Riley KE, Politzer P, Clark T (2010) Directional weak intermolecular interactions: σ -hole bonding. *Aust J Chem* 63:1598–1607
63. Lipkowski P, Grabowski SJ (2014) Could the lithium bond be classified as the σ -hole bond?—QTAIM and NBO analysis. *Chem Phys Lett* 591:113–118
64. Allen FH (2002) The cambridge structural database: a quarter of a million crystal structures and rising. *Acta Cryst B* 58:380–388
65. http://www.ccdc.cam.ac.uk/Lists/ResourceFileList/2014_stats_entries.pdf

66. Domagała M, Grabowski SJ (2009) X-H... π and X-H...N hydrogen bonds—acetylene and hydrogen cyanide as proton acceptors. *Chem Phys* 363:42–48
67. Nishio M, Hirota M, Umezawa Y (1998) The CH/ π interaction, evidence, nature, and consequences. Wiley-VCH, New York
68. Grabowski SJ, Ugalde JM (2010) Bond paths show preferable interactions: ab initio and QTAIM studies on the X-H... π hydrogen bond. *J Phys Chem A* 114:7223–7229
69. Szymczak JJ, Grabowski SJ, Roszak S, Leszczynski J (2004) H... σ interactions—an ab initio and ‘atoms in molecules’ study. *Chem Phys Lett* 393:81–86
70. Grabowski SJ, Sokalski WA, Leszczynski J (2006) Can H... σ , π ...H + ... σ and σ ...H + ... σ interactions be classified as H-bonded? *Chem Phys Lett* 432:33–39
71. Grabowski SJ (2007) Hydrogen bonds with π and σ electrons as the multicenter proton acceptors: high level ab initio calculations. *J Phys Chem A* 111:3387–3393
72. Grabowski SJ (2013) Dihydrogen bond and X-H... σ interaction as sub-classes of hydrogen bond. *J Phys Org Chem* 26:452–459
73. Jucks KW, Miller RE (1987) Infrared stark spectroscopy on the hydrogen-HF binary complex. *J Chem Phys* 87:5629–5633
74. Moore DT, Miller RE (2003) Dynamics of hydrogen–HF complexes in helium nanodroplets. *J Chem Phys* 118:9629–9636
75. Moore DT, Miller RE (2003) Solvation of HF by molecular hydrogen: helium nanodroplet vibrational spectroscopy. *J Phys Chem A* 107:10805–10812
76. Moore DT, Miller RE (2004) Rotationally resolved infrared laser spectroscopy of (H₂)_n-HF and (D₂)_n-HF (n = 2–6) in helium nanodroplets. *J Phys Chem A* 108:1930–1937
77. Bieske EJ, Nizkorodov SA, Bennett FR, Maier JP (1996) The infrared spectrum of the H₂–HCO complex. *J Chem Phys* 102:5152–5164
78. Urban J, Roszak S, Leszczynski J (2001) Shellvation of the ammonium cation by molecular hydrogen: a theoretical study. *Chem Phys Lett* 346:512–518
79. Grabowski SJ, Alkorta I, Elguero J (2013) Complexes between dihydrogen and amine, phosphine, and arsine derivatives. hydrogen bond versus pnictogen interaction. *J Phys Chem A* 117:3243–3251
80. Richardson TB, de Gala S, Crabtree RH (1995) Unconventional hydrogen bonds: intermolecular B-H...H-N interactions. *J Am Chem Soc* 117:12875–12876
81. Wessel J, Lee JC Jr, Peris E, Yap GPA, Fortin JB, Ricci JS, Sini G, Albinati A, Koetzle TF, Eisenstein O, Rheingold AL, Crabtree RH (1995) An unconventional intermolecular three-center N-H...H₂Re hydrogen bond in crystalline [ReH₅(PPh₃)₃]-indole-C₆H₆. *Angew Chem Int Ed Engl* 34:2507–2509
82. Crabtree RH, Siegbahn PEM, Eisenstein O, Rheingold AL, Koetzle TFA (1996) A new intermolecular interaction: unconventional hydrogen bonds with element-hydride bonds as proton acceptor. *Acc Chem Res* 29:348–354
83. Crabtree RH, Eisenstein O, Sini G, Peris E (1998) New types of hydrogen bonds. *J Organomet Chem* 567:7–11
84. Cybulski H, Pecul M, Sadlej J (2003) Characterization of dihydrogen-bonded D-H...H–A complexes on the basis of infrared and magnetic resonance spectroscopic parameters. *J Chem Phys* 119:5094–5104
85. Kubas GJ (2001) Metal dihydrogen and σ -bond complexes. Kluwer, Academic, New York
86. Stephan DW, Erker G (2010) Frustrated Lewis pairs: metal-free hydrogen activation and more. *Angew Chem Int Ed* 49:46–76
87. Rokob TA, Bakó I, Stirling A, Hamza A, Pápai I (2013) Reactivity models of hydrogen activation by frustrated Lewis pairs: synergistic electron transfers or polarization by electric field? *J Am Chem Soc* 135:4425–4437
88. Todd A, Keith TK (2011) AIMAll (Version 11.08.23). Gristmill Software, Overland Park KS, USA (aim.tkgristmill.com)